Electron tunneling into a quantum wire in the Fabry-Perot regime

Electron tunneling into a quantum wire in the Fabry-Pérot regime

Stefano Pugnetti,[1] Fabrizio Dolcini,[1] Dario Bercioux,[2] and Hermann Grabert[2]
[1]*Scuola Normale Superiore and NEST CNR-INFM, I-56126 Pisa, Italy*
[2]*Physikalisches Institut and Freiburg Institute for Advanced Studies, Universität Freiburg, D-79104 Freiburg, Germany*
(Received 19 August 2008; revised manuscript received 5 December 2008; published 26 January 2009)

We study a gated quantum wire contacted to source and drain electrodes in the Fabry-Pérot regime. The wire is also coupled to a third terminal (tip), and we allow for an asymmetry of the tip tunneling amplitudes of right-moving and left-moving electrons. We analyze configurations where the tip acts as an electron injector or as a voltage probe and show that the transport properties of this three-terminal setup exhibit very rich physical behavior. For a noninteracting wire we find that a tip in the voltage-probe configuration affects the source-drain transport in different ways, namely, by suppressing the conductance, by modulating the Fabry-Pérot oscillations, and by reducing their visibility. The combined effect of electron-electron interaction and finite length of the wire, accounted for by the inhomogeneous Luttinger liquid model, leads to significantly modified predictions as compared to models based on infinite wires. We show that when the tip injects electrons asymmetrically the charge fractionalization induced by interaction cannot be inferred from the asymmetry of the currents flowing in source and drain. Nevertheless interaction effects are visible as oscillations in the nonlinear tip-source and tip-drain conductances. Important differences with respect to a two-terminal setup emerge, suggesting new strategies for the experimental investigation of Luttinger liquid behavior.

DOI: 10.1103/PhysRevB.79.035121 PACS number(s): 73.23.Ad, 71.10.Pm, 73.40.Gk

I. INTRODUCTION

Electron scanning of a conductor with a probe terminal is a customary technique to investigate its local properties. The local density of states can be gained from the dependence of the tunneling current on the applied bias. Nowadays, atomically resolved images are obtained both with scanning tunnel microscopes (STMs) and atomic force microscopes (AFMs).[1] So far, most of the efforts of the scientific community have focused on improving the resolution power of the probe terminal. For instance, the recent realization of stable and sharp superconducting STM tips exploits the singularity in the quasiparticle density of states to this purpose.[2] A probe terminal, however, may also be used as a "handle," i.e., as an active component to tune the transport properties of the conductor. Recent works in this direction have shown that the sign of the supercurrent can be changed when a third terminal injects electrons into a Josephson junction under appropriate conditions[3] that the conductance of a quantum dot can be tuned by moving an AFM tip over the sample[4] or that a single-electron transistor can be used to cool down a nanomechanical resonator or to drive it into a squeezed state.[5]

The promising applications of scanning probes in the study of transport properties of nanodevices require a theoretical analysis of electron transport in a three-terminal setup, a subject which has been explored only partly so far. In particular, most of the available investigations are restricted to the case of noninteracting conductors,[6,7] whereas relatively little attention has been devoted to those nanodevices in which electronic correlations play a dominant role. This is the case for one-dimensional (1D) conductors, such as semiconductor heterostructure quantum wires[8] and single-walled carbon nanotubes.[9,10] There, electron-electron interaction dramatically affects the dynamics of charge injection. The response of the system to the scanning probe is quite different from that of ordinary three-dimensional metals since in 1D electronic correlations lead to a breakdown of the Fermi-liquid picture. Semiconductor quantum wires and carbon nanotubes rather exhibit Luttinger liquid (LL) behavior.[11–14] While for this type of systems two-terminal electron transport has been widely analyzed in the last 15 years,[8–14] the electric current and noise in a three-terminal setup, including source and drain electrodes and a tip, have remained mostly unexplored.

There are, however, a few notable works in this direction. The case where a bias is applied between a tip and a semi-infinite LL was investigated by Eggert[15] and by Ussishkin and Glazman.[16] Martin and co-workers[17,18] have recently analyzed the electric noise of the current injected from a tip into a nanotube adiabatically contacted at each end to grounded metallic leads.

In this paper we extend these investigations to a quite general three-terminal setup. We shall thus explore the nonequilibrium current in all three terminals in presence of a transport voltage between the source and drain electrodes, an applied tip voltage, and also a tunable gate voltage. This enables us to address various physical phenomena that are of relevance for recent experiments. Among other effects, we discuss the influence of the tip on the transport along the interacting wire even when no net current is injected from the tip into the wire. In particular, we focus on the Fabry-Pérot transport regime of the wire, which could be recently observed in carbon nanotubes[10,14,19,20] and analyze how Fabry-Pérot oscillations are modified by both the presence of the tip and the electron-electron interaction. To this purpose, the finite length of the wire, the contact resistances at the interfaces between the wire and the side electrodes, as well as an arbitrary position of the tip along the 1D wire are taken into account in our model. Furthermore, inspired by recent experiments on semiconductor quantum wires,[12,21] we allow for an asymmetry in electron tunneling from the tip and investigate how the presence of side electrodes affects the fractionalization of charges injected by the tip into an interacting

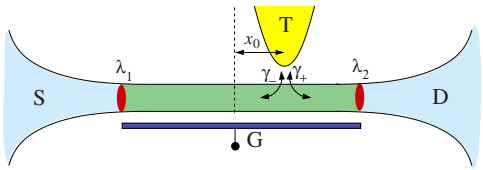

FIG. 1. (Color online) Sketch of the setup. A quantum wire is connected to two metallic electrodes, denoted as source (S) and drain (D) at voltages V_S and V_D, respectively. A third sharp electrode, denoted as tip (T), at voltage V_T, injects electrons into the wire at position x_0. A gate (G) is also present and held at a gate bias voltage V_G. The contact resistances are accounted for by two deltalike scatterers with strengths λ_1 and λ_2, and the electron tunneling amplitudes between the tip and the wire are denoted by $\gamma_\pm$.

wire. Finally, regarding the experimental observation of interaction effects, we discuss the advantages of a three-terminal setup over a two-terminal one.

The paper is organized as follows. In Sec. II we describe the model that we adopt for the setup. In Sec. III we provide results about the electric current in the case of a noninteracting wire, while Sec. IV is devoted to the effects of electron-electron interaction. Finally, we shall discuss the results in Sec. V and present our conclusions. Some more technical details are given in Appendixes A and C.

II. MODEL

We consider a single-channel spinless quantum wire connected, as sketched in Fig. 1, to two metallic electrodes, source (S) and drain (D), as well as to a third sharp electrode, henceforth denoted as tip (T). The wire has a finite length L, and for the x coordinate along it we choose the origin in the middle of the wire so that the interfaces to the S and D electrodes are located at $x_1=-L/2$ and $x_2=+L/2$, respectively. Electron backscattering at the side contacts due to nonadiabatic coupling is modeled by two deltalike scatterers. The tip is described as a semi-infinite noninteracting Fermi liquid, and $y\leq 0$ denotes the coordinate axis along the tip orthogonal to the wire, the origin corresponding to the injection point on the tip. The latter is located at position x_0 with respect to the middle of the wire, and electron injection is modeled by a tunnel Hamiltonian. We also envisage the presence of a metallic gate (G), biased at a voltage V_G. Screening by this gate yields an effectively short-ranged electron-electron interaction potential within the wire, for which the LL model applies.[22–24] The total Hamiltonian of the system reads

$$\mathcal{H} = \mathcal{H}_W + \mathcal{H}_T + \mathcal{H}_{tun}, \tag{1}$$

where the first term describes the wire and its coupling to the S and D electrodes as well as to the gate. The second term accounts for the tip, and the last one describes wire-tip tunneling.

As far as the wire is concerned, we shall address here the low-energy regime, where the wire electron band can be linearized around the Fermi level. Then the wire electron operator $\Psi(x)$ can be decomposed into right-moving and left-moving components $\Psi_+(x)$ and $\Psi_-(x)$,

$$\Psi(x) = e^{+ik_W x}\Psi_+(x) + e^{-ik_W x}\Psi_-(x), \tag{2}$$

where k_W denotes the equilibrium Fermi momentum of the wire. By definition, this is the Fermi momentum in case that the electrochemical potentials of all electrodes, source, drain, tip, and gate, are identical. This corresponds to vanishing applied voltages. Explicitly the Hamiltonian of the wire reads

$$\mathcal{H}_W = \mathcal{H}_{kin,W} + \mathcal{H}_\lambda + \mathcal{H}_{\mu_W} + \mathcal{H}_U. \tag{3}$$

In Eq. (3) the first term,

$$\mathcal{H}_{kin,W} = -i\hbar v_W \int_{-\infty}^{\infty} dx [:\Psi_+^\dagger(x)\partial_x\Psi_+(x): - :\Psi_-^\dagger(x)\partial_x\Psi_-(x):], \tag{4}$$

describes the band energy linearized around the wire Fermi points $\pm k_W$ and characterized by a Fermi velocity v_W. The symbol ": :" stands for normal ordering with respect to the equilibrium ground state. The second term models scatterers at the interfaces[25,26] with the S and D electrodes,

$$\mathcal{H}_\lambda = \hbar v_W \sum_{i=1,2} \lambda_i \rho(x_i), \tag{5}$$

where the dimensionless parameters $\lambda_i \geq 0$ denote the impurity strengths at the contacts x_i, and the term $\rho(x) = :\Psi^\dagger(x)\Psi(x):$ is the electron-density fluctuation with respect to the equilibrium value. The third term in Eq. (3),

$$\mathcal{H}_{\mu_W} = \int_{-\infty}^{+\infty} \mu_W(x)\rho(x)dx, \tag{6}$$

with

$$\mu_W(x) = \begin{cases} eV_S & \text{for } x < -L/2 \\ eV_G & \text{for } -L/2 < x < L/2 \\ eV_D & \text{for } x > L/2, \end{cases} \tag{7}$$

accounts for the bias V_S and V_D of the source and drain electrodes, as well as for the gate voltage V_G. The applied transport voltage is then $V=V_S-V_D$. Finally, the last term,

$$\mathcal{H}_U = \frac{U}{2}\int_{-L/2}^{L/2} dx \sum_{r,r'=\pm} :\rho_r(x)\rho_{r'}(x):, \tag{8}$$

describes the screened Coulomb interaction in the wire,[22,23] where $\rho_r(x) = :\Psi_r^\dagger(x)\Psi_r(x):$ is the density fluctuation of r-moving electrons. As it is customary in LL theory, in the sequel, we characterize the interaction strength by the dimensionless coupling constant,

$$g = \left(1 + \frac{U}{\pi\hbar v_W}\right)^{-1/2}. \tag{9}$$

The Hamiltonian of the tip, the second term in Eq. (1), reads

$$\mathcal{H}_T = \mathcal{H}_{kin,T} + \mathcal{H}_{\mu_T}. \tag{10}$$

Here

$$\mathcal{H}_{\mathrm{kin,T}} = -i\hbar v_{\mathrm{T}} \int_{-\infty}^{\infty} dy{:}c^{\dagger}(y)\partial_y c(y){:} \tag{11}$$

describes the (linearized) band energy with respect to the equilibrium Fermi points $\pm k_{\mathrm{T}}$ of the tip, and v_{T} denotes the Fermi velocity. Notice that the integral runs also over the positive y axis since right-moving and left-moving electron operators along the physical tip axis $y<0$ have been unfolded into one chiral (right-moving) operator $c(y)$ defined on the whole y axis. The second term in Eq. (10) describes the bias V_{T} applied to the tip which affects the incoming electrons according to

$$\mathcal{H}_{\mu_{\mathrm{T}}} = eV_{\mathrm{T}} \int_{-\infty}^{0} dy{:}c^{\dagger}(y)c(y){:}. \tag{12}$$

Finally, the third term in Eq. (1) accounts for the wire-tip electron tunneling and reads

$$\mathcal{H}_{\mathrm{tun}} = \hbar\sqrt{v_{\mathrm{W}}v_{\mathrm{T}}} \sum_{r=\pm} \gamma_r [e^{-ir k_{\mathrm{W}} x_0} \Psi_r^{\dagger}(x_0)c(0) + \mathrm{H.c.}], \tag{13}$$

where γ_r is the dimensionless tunneling amplitude for r-moving electrons, and $x=x_0$ ($y=0$) is the coordinate of the injection point along the wire (tip). Here, we have allowed for an asymmetry of the tip tunneling amplitudes of right-moving and left-moving electrons, which can arise from the presence of a magnetic field.[12,21,27] Note that for $\gamma_+ \neq \gamma_-$ the Hamiltonian is not invariant under time-reversal symmetry.

In Secs. III and IV the electron current will be evaluated in the three terminals of the described setup. Explicitly we shall compute

$$I(x,t) = ev_{\mathrm{W}} \langle {:}\Psi_+^{\dagger}(x,t)\Psi_+(x,t){:} - {:}\Psi_-^{\dagger}(x,t)\Psi_-(x,t){:} \rangle, \tag{14}$$

where x, with $|x|>L/2$, is a measurement point located in the S or D leads. As far as the tip is concerned, due to the unfolding procedure described above, the electron current flowing in the tip at a point $y \leq 0$ acquires the form

$$I(y,t) = ev_{\mathrm{T}} \langle {:}c^{\dagger}(y,t)c(y,t){:} - {:}c^{\dagger}(-y,t)c(-y,t){:} \rangle. \tag{15}$$

In Eqs. (14) and (15) the averages are computed with respect to the stationary state in presence of the applied dc voltages V_{S}, V_{D}, V_{T}, and V_{G}.

Under these conditions, the current in each electrode is actually independent of the measurement point. We thus denote by I_{S} and I_{D} the currents flowing in the source and drain electrodes. The current I_{S} is positive when flowing into the wire, while I_{D} is positive when flowing out of the wire. The current I_{T} flowing in the tip is positive when flowing in the direction of the tip-wire tunnel contact. Current conservation then implies $I_{\mathrm{D}}=I_{\mathrm{S}}+I_{\mathrm{T}}$ so that all currents can be expressed in terms of two independent quantities. One can write

$$I_{\mathrm{S}} = I_{\mathrm{M}} - I_{\mathrm{T}}/2, \tag{16}$$

$$I_{\mathrm{D}} = I_{\mathrm{M}} + I_{\mathrm{T}}/2, \tag{17}$$

where I_{M} describes the current flowing in the wire under the condition that no net current flows through the tip (voltage probe configuration). Importantly, I_{M} should *not* be identified with the two-terminal current flowing in the absence of the tip. Indeed, while $\gamma_{\pm}=0$ implies that $I_{\mathrm{T}}=0$, the opposite does not hold so that I_{M} needs to be evaluated by accounting for the whole three-terminal setup.

III. NONINTERACTING CASE

In this section we first discuss results for the case that the electron interaction [Eq. (8)] is neglected. Then Hamiltonian (1) of the whole system is quadratic in the fields $\Psi_{\pm}(x)$ and $c(y)$, and transport properties can be determined within the Landauer-Büttiker formalism. In the three-terminal setup that we are considering, the scattering matrix $\mathbf{S}(E)$ is a 3×3 matrix which depends on the energy E measured with respect to the equilibrium wire-lead Fermi level. The currents I_{M} and I_{T} defined through Eqs. (16) and (17) read as

$$\begin{aligned} I_{\mathrm{M}} = \frac{e}{h}\Bigg\{ & \frac{1}{2}\int_{-\infty}^{\infty} (|\mathbf{S}_{12}|^2 + |\mathbf{S}_{21}|^2)[f_{\mathrm{S}}(E) - f_{\mathrm{D}}(E)]dE \\ & + \frac{1}{2}\int_{-\infty}^{\infty} |\mathbf{S}_{13}|^2 [f_{\mathrm{S}}(E) - f_{\mathrm{T}}(E)]dE \\ & + \frac{1}{2}\int_{-\infty}^{\infty} |\mathbf{S}_{23}|^2 [f_{\mathrm{T}}(E) - f_{\mathrm{D}}(E)]dE \Bigg\}, \end{aligned} \tag{18}$$

and

$$I_{\mathrm{T}} = \frac{e}{h}\int_{-\infty}^{\infty} dE\{|\mathbf{S}_{31}|^2[f_{\mathrm{T}}(E) - f_{\mathrm{S}}(E)] + |\mathbf{S}_{32}|^2[f_{\mathrm{T}}(E) - f_{\mathrm{D}}(E)]\}. \tag{19}$$

In the $\mathbf{S}$-matrix elements appearing in Eqs. (18) and (19) the source, drain, and tip electrodes are identified as 1, 2, and 3, respectively, whereas their Fermi functions are denoted as f_{S}, f_{D}, and f_{T}. Note that the $\mathbf{S}$-matrix is in general not symmetric because time-reversal symmetry is broken for $\gamma_+ \neq \gamma_-$. The $\mathbf{S}$-matrix can straightforwardly be evaluated with standard techniques by combining the transfer matrices $\mathbf{M}_{x_i}$ ($i=1,2$) of the two side contacts,

$$\mathbf{M}_{x_1,x_2} = \begin{pmatrix} e^{-iu_{\mathrm{G}}/2}(1 - i\lambda_{1,2}) & \pm ie^{\pm i(2\varepsilon - u_{\mathrm{G}} + 2\kappa_{\mathrm{W}})/2}\lambda_{1,2} & 0 \\ ie^{\mp i(2\varepsilon - u_{\mathrm{G}} + 2\kappa_{\mathrm{W}})/2}\lambda_{1,2} & e^{iu_{\mathrm{G}}/2}(1 + i\lambda_{1,2}) & 0 \\ 0 & 0 & 1 \end{pmatrix}, \tag{20}$$

with the one, $\mathbf{M}_{x_0}$, at the tip injection point,

$$\mathbf{M}_{x_0} = \frac{1}{1+(\gamma_+^2-\gamma_-^2)/4}\begin{pmatrix} 1-(\gamma_+^2+\gamma_-^2)/4 & -e^{-2i(\varepsilon+\kappa_W-u_G)\xi_0}\gamma_+\gamma_-/2 & -ie^{-i(\varepsilon+\kappa_W-u_G)\xi_0}\gamma_+ \\ e^{2i(\varepsilon+\kappa_W-u_G)\xi_0}\gamma_+\gamma_-/2 & 1+(\gamma_+^2+\gamma_-^2)/4 & ie^{i(\varepsilon+\kappa_W-u_G)\xi_0}\gamma_- \\ -ie^{i(\varepsilon+\kappa_W-u_G)\xi_0}\gamma_+ & -ie^{-i(\varepsilon+\kappa_W-u_G)\xi_0}\gamma_- & 1-(\gamma_+^2-\gamma_-^2)/4 \end{pmatrix}. \tag{21}$$

Here, we have introduced the ballistic frequency,

$$\omega_L = \frac{v_F}{L}, \tag{22}$$

associated with the length of the wire, and the following dimensionless quantities:

$$\xi_0 = \frac{x_0}{L}, \tag{23a}$$

$$\kappa_W = k_W L, \tag{23b}$$

$$u_G = \frac{eV_G}{\hbar\omega_L}, \tag{23c}$$

$$\varepsilon = \frac{E}{\hbar\omega_L}. \tag{23d}$$

The scattering matrix is obtained as a combination of the elements of the transmission matrix $\mathbf{M}=\mathbf{M}_{x_2}\mathbf{M}_{x_0}\mathbf{M}_{x_1}$ in the form,

$$\mathbf{S} = \mathbf{M}_{22}^{-1} \times \begin{pmatrix} -\mathbf{M}_{21} & 1 & -\mathbf{M}_{23} \\ \mathbf{M}_{11}\mathbf{M}_{22}-\mathbf{M}_{12}\mathbf{M}_{21} & \mathbf{M}_{12} & \mathbf{M}_{13}\mathbf{M}_{22}-\mathbf{M}_{12}\mathbf{M}_{23} \\ \mathbf{M}_{31}\mathbf{M}_{22}-\mathbf{M}_{21}\mathbf{M}_{32} & \mathbf{M}_{32} & \mathbf{M}_{33}\mathbf{M}_{22}-\mathbf{M}_{23}\mathbf{M}_{32} \end{pmatrix}, \tag{24}$$

where $\mathbf{M}_{ij}$ are the matrix elements of $\mathbf{M}$.

A. Fabry-Pérot oscillations in a two-terminal setup

Before discussing the influence of the STM tip, we shortly describe the transport properties in the absence of the tip, i.e., for $\gamma_\pm=0$. In this case we have a two-terminal setup with $I_T=0$ and $I_S=I_D=I_M$. The solid line in Fig. 2 shows the two-terminal conductance dI_M/dV at zero temperature plotted in units of e^2/h as a function of the (dimensionless) source-drain bias,

$$u = \frac{e(V_S-V_D)}{\hbar\omega_L}, \tag{25}$$

for identical contact impurity strengths $\lambda_1=\lambda_2$. For $\lambda_i \ll 1$ the conductance shows the typical Fabry-Pérot oscillations with maximum values close to one. For carbon nanotubes the Fabry-Pérot regime of highly transparent contacts could be reached experimentally only recently due to progress achieved in device contacting.[10,14,19,20] In the sequel, we will focus on this regime.

The electron current $I_S=I_D=I_M$ can be written as

$$I_M = I_0 + I_{imp}, \tag{26}$$

where $I_0=(e^2/h)V$ represents the current of a perfectly contacted wire, and I_{imp} characterizes the (negative) correction due to the contact resistances. The exact expression for I_{imp}, which can be gained from the **S** matrix, is not easily tractable for arbitrary impurity strengths and temperature. In the Fabry-Pérot regime at zero temperature, however, a simpler expression is obtained by expanding in terms of the impurity strengths. To third order in the λ_i's one obtains

$$I_{imp} = \frac{e\omega_L}{2\pi}(j_{inc}+j_{coh}), \tag{27}$$

where j_{inc} and j_{coh} are the dimensionless quantities describing the incoherent and coherent contributions, respectively, to the reduction in the current caused by the contact impurities. The term

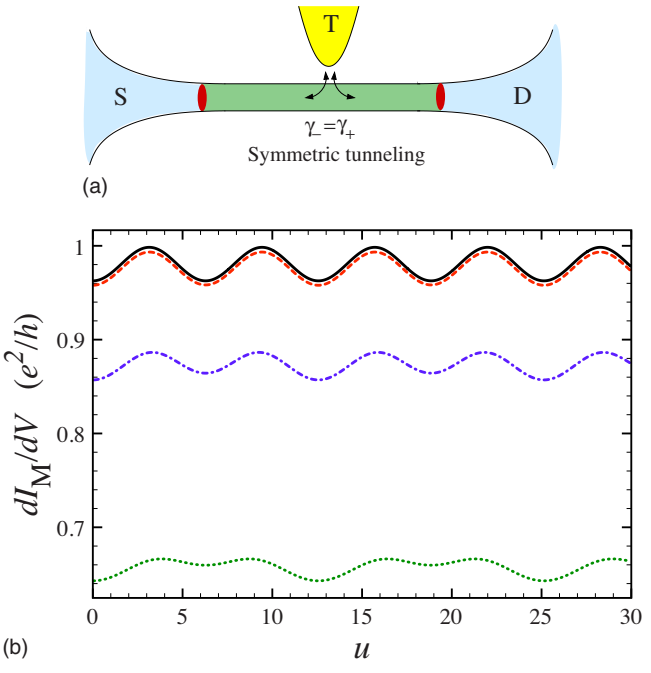

FIG. 2. (Color online) Zero-temperature differential conductance as a function of the source-drain bias for a noninteracting wire characterized by contact impurity strengths $\lambda_1=\lambda_2=0.1$ and a Fermi wave vector $\kappa_W=0.3$. The tip is located in the middle of the wire and the tip voltage V_T is adjusted to fulfill the condition $I_T=0$. Tunneling is symmetric ($\chi=0$), and the tunneling strength has the values: $\gamma=0$ (solid line), $\gamma=0.1$ (dashed-line), $\gamma=0.5$ (dashed-dotted line), and $\gamma=1$ (dotted line). The gate is grounded ($V_G=0$), and the bias is applied symmetrically ($V_{S/D}=\pm V/2$).

$$j_{\rm inc} = -\sum_{i=1,2} \lambda_i^2 u \tag{28}$$

is linear in the applied bias voltage, and the coefficient of proportionality is the "classical" series resistance of two impurities. In contrast, the term $j_{\rm coh}$ stems from quantum interference between scattering processes. This interference leads to the Fabry-Pérot oscillations of $j_{\rm coh}$. Explicitly,

$$j_{\rm coh} = j_{\rm coh}^{(2)} + j_{\rm coh}^{(3)}, \tag{29}$$

where

$$j_{\rm coh}^{(2)} = -2\lambda_1\lambda_2 \cos[2(u_{\rm W} + \kappa_{\rm W} - u_{\rm G})]\sin(u), \tag{30}$$

and

$$j_{\rm coh}^{(3)} = -2(\lambda_1\lambda_2^2 + \lambda_1^2\lambda_2)\sin[2(u_{\rm W} + \kappa_{\rm W} - u_{\rm G})]\sin(u), \tag{31}$$

where we have introduced

$$u_{\rm W} = \frac{e(V_{\rm S} + V_{\rm D})}{2\hbar\omega_L}. \tag{32}$$

From Eqs. (30) and (31) one can see that Fabry-Pérot oscillations arise both as a function of the source-drain bias u and as a function of the gate voltage $u_{\rm G}$. Note that for a noninteracting system the period in the former case is twice as large as the period in the latter case.

We also emphasize that $j_{\rm coh}^{(3)}$ originates from impurity forward-scattering processes (more precisely from second order in backward scattering and first order in forward scattering). Forward-scattering processes are typically neglected in single impurity problems, where they can be gauged away. However, when two or more impurities are present they affect the coherent part of transport. Although this contribution is in general smaller than $j_{\rm coh}^{(2)}$, it becomes the dominant term for the Fabry-Pérot oscillations when $j_{\rm coh}^{(2)}$ vanishes, which is the case for

$$\frac{4}{\pi}\left(k_{\rm W}L + \frac{e(V_{\rm S} + V_{\rm D} - 2V_{\rm G})}{2\hbar\omega_L}\right) \simeq \text{odd integer}. \tag{33}$$

Thus, the third-order term is crucial for certain values of the biasing voltage.

We conclude the discussion of the two-terminal case by emphasizing that for a noninteracting wire in the Fabry-Pérot regime the current depends not only on the difference $V_{\rm S} - V_{\rm D}$, but in general on $V_{\rm S}$ and $V_{\rm D}$ separately. This is simply due to the fact that Fabry-Pérot interference effects lead to an energy-dependent transmission coefficient and, hence, to nonlinearity in the applied bias. Notice that Eqs. (28), (30), and (31) fulfill the gauge-invariance condition emphasized by Büttiker[28] since they are invariant under an overall shift of the potentials $V_p \to V_p + \text{const}$ $(p = \text{S}, \text{D}, \text{G})$.

B. Effect of the tip on Fabry-Pérot oscillations

In this section we shall address, within the noninteracting electron approximation, the effect of the STM tip on the Fabry-Pérot oscillations. When $\gamma_\pm \neq 0$, the currents $I_{\rm M}$ and $I_{\rm T}$ are nonvanishing for arbitrary values of the applied voltages $V_{\rm S}$, $V_{\rm D}$, and $V_{\rm T}$. We analyze the effects of the tip as a function of the total tunneling strength γ, defined through

$$\gamma^2 = \frac{\gamma_+^2 + \gamma_-^2}{2}, \tag{34}$$

the tunneling asymmetry coefficient,

$$\chi = \frac{\gamma_+^2 - \gamma_-^2}{\gamma_+^2 + \gamma_-^2} \quad |\chi| \leq 1, \tag{35}$$

and the position x_0 of the tip.

We start by considering the situation where the tip behaves as an electron injector: a bias is applied between the tip and the source and drain electrodes, which, for simplicity, are assumed to be at the same electrochemical potential. A quite standard calculation applies to the case of fully symmetric tunneling ($\chi = 0$), allowing, e.g., to relate the local density of states in the wire to the nonlinear conductance as a function of the tip-wire bias. Here, we shall instead focus on the case of fully asymmetric tunneling ($\chi = \pm 1$), which has become of particular interest due to recent experiments where only right-moving or only left-moving electrons could be selectively tunneled into a semiconductor quantum wire due to the presence of a magnetic field normal to the plane of the wire and the tip.[21] We find that novel physical aspects emerge from a tunneling asymmetry. In the first instance, a direct inspection of the scattering matrix [Eq. (24)] shows that its elements $\mathbf{S}_{ij}$ are independent of x_0, implying that, differently from the case of symmetric tunneling $\chi = 0$, the lead currents $I_{\rm D}$ and $I_{\rm S}$ *do not* depend on the position of the tip. Furthermore, asymmetric tunneling can be used to extract the transmission coefficient of each contact. Indeed evaluating the asymmetry,

$$\mathcal{A}(\chi) \doteq \left.\frac{|I_{\rm D}| - |I_{\rm S}|}{|I_{\rm D}| + |I_{\rm S}|}\right|_\chi, \tag{36}$$

between $I_{\rm D}$ and $I_{\rm S}$ in the two cases of totally asymmetric injection only to the right ($\chi = 1$) and only to the left ($\chi = -1$), one obtains

$$\mathcal{A}_+ = \frac{1 + \lambda_1^2 - \lambda_2^2}{1 + \lambda_1^2 + \lambda_2^2} \tag{37}$$

and

$$\mathcal{A}_- = \frac{1 + \lambda_2^2 - \lambda_1^2}{1 + \lambda_1^2 + \lambda_2^2}, \tag{38}$$

where $\mathcal{A}_\pm = \pm\mathcal{A}(\pm 1)$. From these coefficients it is straightforward to extract the strengths of the contact impurities,

$$\lambda_1^2 = \frac{1 - \mathcal{A}_-}{\mathcal{A}_+ + \mathcal{A}_-},$$

$$\lambda_2^2 = \frac{1 - \mathcal{A}_+}{\mathcal{A}_+ + \mathcal{A}_-}, \tag{39}$$

as well as the transmission coefficients,

$$\mathcal{T}_{1,2} \doteq \frac{1}{1+\lambda_{1,2}^2} = \frac{\mathcal{A}_+ + \mathcal{A}_-}{1+\mathcal{A}_\pm}, \tag{40}$$

related to each of the two contacts.

Notice that, while I_S and I_D depend on the temperature T, Eqs. (37) and (38) are independent of T within the approximation of a linearized band. Interestingly, these equations also enable one to identify the relation between the current asymmetry coefficients $\mathcal{A}_\pm$ and the two-terminal conductance $G_{2t}=\partial I_M/\partial V|_{\gamma=0}$. In Ref. 27, the equality $\mathcal{A}_\pm = G_{2t}/(e^2/h)$ is claimed to hold for a setup with symmetric contacts to the leads even in the presence of interactions. However, Eqs. (37) and (38) show that for a quantum wire in the Fabry-Pérot regime even in the absence of interactions and with perfectly symmetric contacts $\lambda_1=\lambda_2$, one has

$$\mathcal{A}_+ = \mathcal{A}_- \neq G_{2t}/(e^2/h) \tag{41}$$

since $\mathcal{A}_\pm = 1/(1+2\lambda_1^2)$ is a constant, whereas G_{2t} depends on temperature, source-drain bias, and gate voltage. The equality sign in Eq. (41) holds only under the specific circumstances of perfectly transmitting contacts ($\lambda_{1,2}=0$), or of a perfectly symmetric setup ($\lambda_1=\lambda_2\neq 0$) at sufficiently high temperatures $k_BT \gg \hbar\omega_L$, where Fabry-Pérot oscillations of G_{2t} wash out.

The second situation that we want to investigate is when the tip voltage V_T is set to an appropriate value $\bar{V}_T$ so that no net current flows through the tip. This corresponds to a situation where the tip behaves as a voltage probe.[29] Notice that, even under the condition $I_T=0$, electrons can tunnel from the tip to the wire and vice versa, and therefore the tip *does* affect the electron transport between source and drain.

We start by describing the case of symmetric tunneling ($\chi=0$) with the tip located in the middle of the wire ($x_0=0$). The differential conductance dI_M/dV, evaluated under the condition $I_T=0$, is depicted in Fig. 2 as a function of the source-drain bias [Eq. (25)], for different values of γ, ranging from weak to strong tunneling. The tip has three main effects on the Fabry-Pérot oscillations: (i) an overall suppression of the conductance, (ii) a modulation of the maxima and minima, and (iii) a reduction in the visibility of the oscillations.

The origin of the first effect can be illustrated already in the case of a clean wire ($\lambda_i=0$), where it is easy to show that the condition $I_T=0$ is fulfilled for a tip voltage $\bar{V}_T=(V_S+V_D)/2$, and that

$$I_M = \frac{e^2}{h}\frac{V_S - V_D}{1+\gamma^2/2} < \frac{e^2}{h}(V_S - V_D). \tag{42}$$

Notice that a reduction in the conductance already shows up to order γ^2 in the tunneling strength. The reason for this suppression of the current is that a fraction of the electron flow originating from the source is diverted into the tip due to the tip-wire coupling. While the condition $I_T=0$ ensures that the same electron current is reinjected into the wire, for symmetric tunneling the tip injects (with equal probabilities) both right-moving and left-moving electrons. Hence half of the injected current flows back to the source electrode, causing the reduction in the two-terminal conductance. As we shall see below, the situation is different in the case of asymmetric tunneling.

The second feature that can be observed in Fig. 2 is an alternating depth of the Fabry-Pérot minima. This modulation originates from the interference between different paths that are possible for an electron ejected from the tip. For instance, the path of an electron ejected as right mover toward the drain can interfere with the path starting as left mover toward the source followed by an elastic backscattering at the source contact. The difference in length between these paths corresponds to a new frequency in the oscillations, which causes the modulation of the peaks. In the case of Fig. 2, where the tip is located in the middle, this additional frequency equals twice the Fabry-Pérot frequency so that the tip affects every second minimum in the same way. As we shall see below, in general, the modulation pattern depends both on the asymmetry coefficient and on the position of the tip. The modulation effect arises to order $\gamma^2\lambda$ when we treat the impurity strength and tunneling amplitudes as perturbation parameters.

The third effect of the tip consists in a reduction in the visibility of the Fabry-Pérot oscillations: in the presence of the tip the relative separation between maxima and minima decreases. This reduction stems from the decoherence introduced by the tip since the probability of constructive interference between paths with two backscattering processes at the contacts decreases when electrons can be incoherently absorbed and re-ejected by the tip. Notice that the reduction in visibility is of order of $\gamma^2\lambda^2$, and it is therefore negligible with respect to the modulation effect in the Fabry-Pérot regime.

Let us now discuss the role of asymmetric tunneling in the voltage-probe configuration. When $\chi\neq 0$, the effect of conductance suppression is less pronounced then for symmetric tunneling. This can be seen already in the case of a clean wire ($\lambda_i=0$), where

$$I_M = \frac{e^2}{h}(V_S - V_D)\frac{2+\gamma^2\chi^2}{2+\gamma^2}, \tag{43}$$

and the value $\bar{V}_T$ of the tip voltage ensuring $I_T=0$ is given by

$$\bar{V}_T = \frac{1}{2}[V_S(1+\chi) + V_D(1-\chi)]. \tag{44}$$

As one can see from the last factor in Eq. (43), the suppression of the current I_M is completely absent for fully asymmetric tunneling $\chi=\pm 1$. Importantly, this feature persists also in the presence of realistic contacts ($\lambda_i\neq 0$), as shown in Fig. 3, where the differential conductance dI_M/dV is plotted as a function of the source-drain voltage for several values of the tunneling strength γ. Increasing the tunneling strength simply decreases the amplitude of the Fabry-Pérot oscillations but does not change the average value of the conductance. Two more noteworthy features can be observed: in the fully asymmetric case also the modulation of the peaks is absent, and the nonlinear conductance is independent of the tip position. The reason lies in the specific tunneling conditions. For example, a right-moving electron ejected by the tip cannot be readsorbed after scattering as a left-moving one,

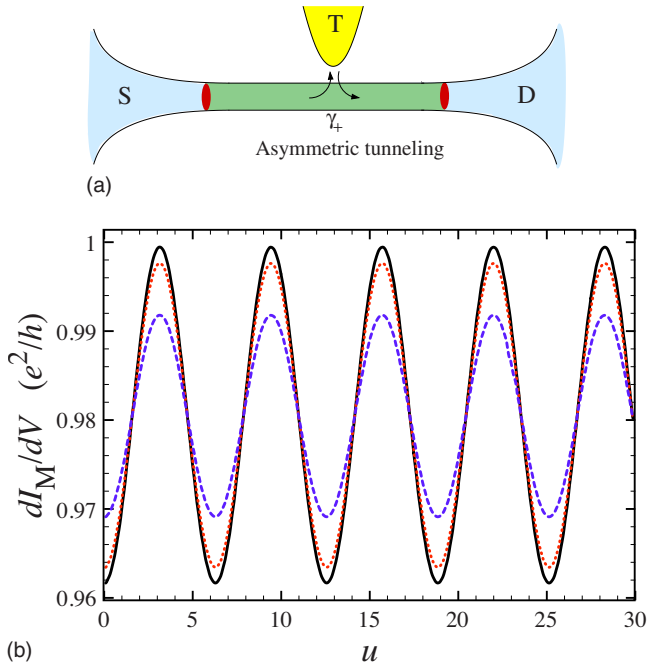

FIG. 3. (Color online) Zero-temperature differential conductance as a function of the source-drain bias for a noninteracting wire with contact impurity strengths $\lambda_1=\lambda_2=0.1$ in presence of a tip with an applied voltage V_T adjusted to fulfill the condition $I_T=0$. Tunneling is totally asymmetric ($\chi=1$), and the tunneling strength has the values $\gamma=0.3$ (dotted line) and $\gamma=0.7$ (dashed line). The solid line represents the case with $\gamma=0$. The result is independent of the tip position x_0. The gate is grounded ($V_G=0$), and the bias is applied symmetrically ($V_{S/D}=\pm V/2$).

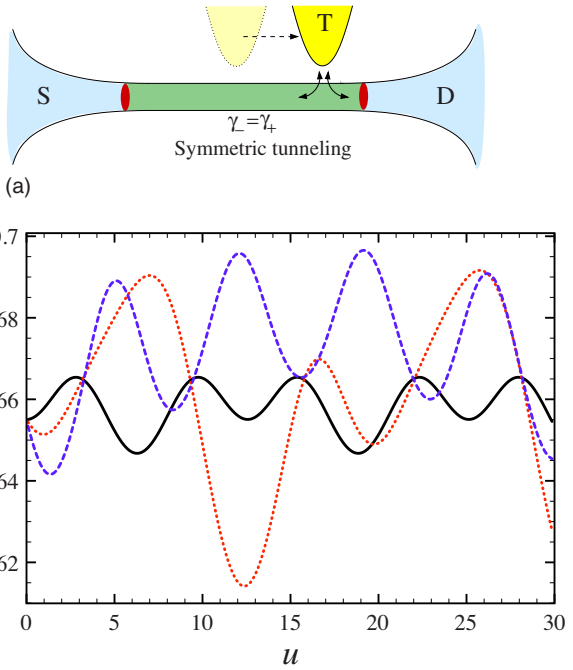

FIG. 4. (Color online) Zero-temperature differential conductance as a function of the source-drain voltage for a noninteracting wire for several values of the tip position $x_0=0$ (solid line), $x_0=0.17$ (dotted line), and $x_0=0.41$ (dashed line). Tunneling has amplitude $\gamma=1$ and is symmetric ($\chi=0$). The contact impurities have equal strengths $\lambda_1=\lambda_2=0.1$. The gate is grounded ($V_G=0$), and the bias is applied symmetrically ($V_{S/D}=\pm V/2$).

and this rules out interference effects between electrons traveling through the tip and electrons that have undergone an odd number of backscattering events at the contacts. Such processes would give rise to effects related to the tip position, while interference phenomena with electrons that have undergone an even number of backscattering events, which continue to be present also for $\chi=\pm 1$, are independent of the tip position. Moreover, in the completely asymmetric case, electrons passing through the tip continue to move in the same direction, and this is the reason why, also for strong tunneling, the average value of the differential conductance is independent of γ.

Finally, we analyze the dependence of the differential conductance on the tip position. For simplicity we limit this discussion to the case of symmetric tunneling illustrated in Fig. 4. Apart from the conductance suppression discussed above, one sees that the modulation effect exhibits a strong dependence on the tip position. In particular, when the tip is close to a contact impurity, we observe Fabry-Pérot-type oscillations overimposed by an oscillation with large period due to coherent motion of carriers between the tip and the contact impurity remote from the tip.

IV. INTERACTING CASE

In this section we discuss the three-terminal setup in presence of electron-electron interaction. For arbitrary values of the interaction strength, contact resistances, and tunneling amplitudes an analytical treatment is not possible, therefore we focus here on the Fabry-Pérot regime. In this regime, characterized by highly transparent contacts to the electrodes, the role of interactions has so far only been analyzed for a two terminal setup.[25,26] Since the impurity strengths λ_i are small, they can be treated perturbatively. The electron-electron interaction [Eq. (8)] will be accounted for exactly using bosonization. The evaluation of the currents in the three terminals will be based on the out-of-equilibrium Keldysh formalism.[30] We shall first discuss the effects of electron-electron interaction for the two-terminal setup in the Fabry-Pérot regime, i.e., in the absence of the tip, and then turn to the combined effect of tip and electronic correlations.

A. Interaction effects on Fabry-Pérot oscillations in a two-terminal setup

Let us first analyze the effects of electron-electron interaction for a contacted wire without tip. As in the noninteracting case, for $\gamma_\pm=0$ the problem is reduced to a two-terminal setup, where $I_T=0$ and $I_S=I_D=I_M$. Furthermore, I_M can again be written as a sum of the current I_0 in a wire with adiabatic contacts and I_{imp}, see Eq. (26). Importantly, while I_0 is unaffected by the interaction in the wire,[22,23] the current I_{imp}, accounting for the contact resistances, is strongly modified by the interaction. One can still decompose I_{imp} into

$$I_{\rm imp} = \frac{e\omega_L^*}{2\pi}(j_{\rm inc} + j_{\rm coh}), \tag{45}$$

where $j_{\rm inc}$ is the sum of two terms related to a single impurity each and $j_{\rm coh}$ describes the interference between scattering processes at the two impurities. Here, an important difference emerges with respect to the noninteracting case. The Fermi velocity *in the wire* is enhanced by the interaction parameter g, leading to a higher ballistic frequency,

$$\omega_L^* = \frac{\omega_L}{g}. \tag{46}$$

Moreover, the interaction is also affecting the strength of the contact impurities: the forward-scattering processes are left unchanged, whereas the backscattering ones are renormalized,[31]

$$\lambda \to \begin{cases} \lambda_{B,i}^* = \lambda \alpha_{\rm W}^{g-1}, \\ \lambda_{F,i} = \lambda, \end{cases} \tag{47}$$

where $\alpha_{\rm W}=a_{\rm W}/gL$ is a small dimensionless cut-off parameter. The cut-off length $a_{\rm W}$, which is related to the lattice spacing or the electronic bandwidth of order of $\hbar v_{\rm W}/a_{\rm W}$, is introduced in Appendix B.

In the Fabry-Pérot regime we can again restrict ourselves to terms up to third order in the contact impurity strengths λ_i. Then, the incoherent and the coherent contributions can be written as

$$j_{\rm inc} = \sum_{i=1,2} j_{{\rm inc},i}, \tag{48}$$

and

$$j_{\rm coh} = j_{\rm coh}^{(2)} + j_{\rm coh}^{(3)}, \tag{49}$$

with

$$j_{{\rm inc},i} = (\lambda_{B,i}^*)^2 D_{ii}(u), \tag{50}$$

and

$$j_{\rm coh}^{(2)} = 2\lambda_{B,1}^*\lambda_{B,2}^* D_{12}(u)\cos\{2[\kappa_{\rm W} + g(u_{\rm W} - u_{\rm G})]\}, \tag{51}$$

$$j_{\rm coh}^{(3)} = 2\lambda_{B,1}^*\lambda_{B,2}^*(\lambda_{F,1} + \lambda_{F,2}) D_{12}(u) \times g^2 \sin\{2[\kappa_{\rm W} + g(u_{\rm W} - u_{\rm G})]\}, \tag{52}$$

where we have introduced

$$D_{ij}(u) = \frac{2}{\pi\alpha_{\rm W}^{2g}} \int_0^\infty d\tau \sin(u\tau) \times \sin[4\pi \mathcal{I}^{\Phi\Phi}(\xi_i;\xi_j;\tau)] e^{4\pi \mathcal{R}_{\rm reg}^{\Phi\Phi}(\xi_i;\xi_j;\tau)}. \tag{53}$$

The dimensionless voltages u, $u_{\rm W}$, and $u_{\rm G}$ are now scaled by the factor $e/\hbar\omega_L^*$ compared to the physical voltages $V_{\rm S}-V_{\rm D}$, $(V_{\rm S}+V_{\rm D})/2$, and $V_{\rm G}$, respectively. In the expression for D_{ij}, the dimensionless integration time is defined as $\tau=\omega_L^* t$, and the functions $\mathcal{R}_{\rm reg}^{\Phi\Phi}(\xi;\xi';\tau)$ and $\mathcal{I}^{\Phi\Phi}(\xi;\xi';\tau)$ are the real and imaginary parts, respectively, of the autocorrelation function of the bosonic phase field Φ introduced in Appendix B. The quantity D_{ij} defined in Eq. (53) is cut-off independent since the cut-off dependence of the prefactor is compensated by the correlation functions. Explicit results for the phase field autocorrelation function have been given in a previous paper.[32] Further, the $\xi_i=x_i/L$ $(i=1,2)$ are dimensionless contact impurity positions. Equations (50)–(52) are obtained from a perturbative development of the current in the impurity strengths λ_i employing the methods described in Appendixes A and B. The current $j_{\rm coh}^{(3)}$ in Eq. (52) includes forward-scattering processes that give rise to the factor $\lambda_{F,1}+\lambda_{F,2}$ and a twofold backscattering contribution leading to the factor $\lambda_{B,1}^*\lambda_{B,2}^*$.

Another important effect of the interaction is that the incoherent term $j_{\rm inc}$ does not depend linearly on the bias as in the noninteracting case. Instead, it exhibits oscillations of period $\Delta u=\pi$ due to the interplay between backward scattering at one contact impurity and Andreev-type reflection at the other contact.[32] On the other hand, the coherent term $j_{\rm coh}$ responsible for Fabry-Pérot oscillations shows a power-law suppression with increasing voltage.[25,26] Thus, in the presence of interaction two types of oscillations are present, namely, the Fabry-Pérot ones (already existing for a noninteracting wire and modified by the interaction) and the Andreev-type ones (purely due to the interaction). These two types of oscillations are characterized by the same period in the source-drain bias, and they are of the same order in the impurity strength if we assume that the two contact transparencies are comparable $(\lambda_1 \simeq \lambda_2)$. It is therefore difficult to distinguish the two phenomena from an inspection of the two-terminal differential conductance, which is shown in Fig. 5 as a function of the source-drain bias for various values of the interaction parameter g. Besides the power-law suppression of the amplitude at high applied bias, we see that for strong interaction $(g<1/2)$ the sinusoidal behavior of the oscillations is deformed into a sawtoothlike shape. Furthermore, although the total current [Eq. (26)] in the presence of contact resistances is always smaller than the current I_0 of an ideally contacted wire $(I_{\rm imp}\leq 0)$, the differential conductance may exceed e^2/h. This is a well-known effect of nonlinear transport in Luttinger liquids,[33] reflecting the fact that the conductance cannot be expressed in terms of single-particle transmission coefficients. In Sec. V we shall comment on how the two types of oscillations may be experimentally distinguished in a three-terminal setup.

Further interesting insights emerge from the analysis of the conductance $dI_{\rm M}/dV$ as a function of both the source-drain bias $V=V_{\rm S}-V_{\rm D}=(\hbar\omega_L^*/e)u$ and the gate bias $V_{\rm G}=(\hbar\omega_L^*/e)u_{\rm G}$. Corresponding conductance plots are shown in Fig. 6. Panels (a), (b), and (c) refer to three different values of the interaction strength g, in the case of a symmetrically applied source-drain bias, $u_{\rm S/D}=\pm u/2$. The oscillations of the conductance as a function of V and $V_{\rm G}$ are characterized by two periods ΔV and $\Delta V_{\rm G}$. The period ΔV coincides with the period of the function $D_{12}(u)$ [Eq. (53)] appearing in the coherent terms [Eqs. (51) and (52)] since the functions $D_{11}(u)$ and $D_{22}(u)$ related to the incoherent contribution [Eq. (50)] exhibit the period $\Delta V/2$. We thus recover the result of Ref. 26. On the other hand, the period $\Delta V_{\rm G}$ in the gate voltage is determined by the sinusoidal factors of Eqs. (51) and (52). The values of ΔV and $\Delta V_{\rm G}$ depend on the interaction strength g and are inversely proportional to g and g^2, respec-

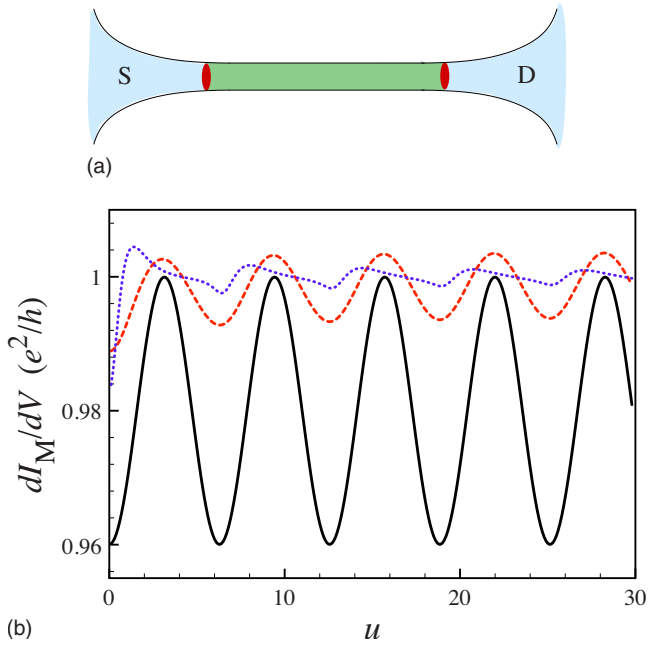

FIG. 5. (Color online) Differential conductance of the two-terminal setup (in the absence of a tip) as a function of the source-drain voltage for several values of the interaction parameter $g=1$ (solid line), $g=0.75$ (dashed line), and $g=0.25$ (dotted line). The contact impurities have equal strengths $\lambda^*_{B,1}=\lambda^*_{B,2}=0.1$. The gate voltage is $V_G=0$, and the bias is applied symmetrically $(V_{S/D}=\pm V/2)$.

tively. Interestingly, the ratio of these periods yields the Luttinger liquid interaction strength, $\Delta V/\Delta V_G=\Delta u/\Delta u_G=2g$, as can be checked from the table associated with Fig. 6.

Panel (d) describes the case of an asymmetrically applied bias ($u_S=u$ and $u_D=0$) for the same interaction strength as panel (b). In this case $u_W=u/2$ [see Eq. (32)] so that an additional dependence on V arises from the sinusoidal factors of Eqs. (51) and (52), and the period in V at fixed V_G changes. For this reason the two-dimensional pattern of the nonlinear conductance is twisted with respect to panel (b). However, the quantities ΔV and ΔV_G related to a symmetrically applied bias can still be obtained, e.g., by projecting the conductance maxima on the V axis and measuring the distance between these projections as indicated by the arrows in panel (d). The value of g can therefore be extracted also in this case as $\Delta u/\Delta u_G=2g$. We remark that a qualitatively similar twist of the conductance pattern has recently been observed in carbon nanotubes.[19]

Conductance plots as a function of the transport and gate voltages have previously been discussed in the context of carbon nanotubes in Refs. 25 and 26. We point out that the way we introduce the bias and gate voltages in our model [see Eq. (6)] differs from the one adopted in the above papers. Our approach accounts for several basic physical facts. In a nonchiral quantum wire only the electrochemical potentials of the leads can be controlled experimentally, whereas the electrochemical potentials of right and left movers inside the wire are a result of the biasing of the wire and its screening properties. As a consequence, the source and drain biases, V_S and V_D, are applied here only in the related leads. This is in accord with a basic hypothesis underlying the definition of an electrode, namely, that inelastic processes in the lead equilibrate absorbed electrons, yielding a voltage drop at the contacts *even* in the absence of contact impurities. On the other hand, the charge density of metallic electrodes is typically insensitive to a gate due to their electroneutrality. For this reason, in our model the gate voltage V_G is applied only to the interacting wire and not to the leads.

The precise form of the coupling to the biasing voltages adopted in the model has implications on the behavior of the current as a function of bias and gate voltages. We find that the dependence on V_G and $(V_S+V_D)/2$ involves a factor g^2, as shown, for instance, in Eqs. (51) and (52). (In the dimensionless formulation one factor of g is contained in the definition of the dimensionless quantities u_G and u_W.) The difference $(V_S+V_D)/2-V_G$ is proportional to the *bare* electron charge injected into the wire, whereas the g^2 factor originates from the partial screening occurring in a Luttinger liquid[34] and physically describes the fraction of the bare charge that remains unscreened. In particular, in the limit $g\to 0$ of an electroneutral wire we obtain that the current depends only on the difference V_S-V_D and is independent of the gate, as it should be.

On a more formal level, these physical properties are encoded in the zero modes $\Phi_{0,\pm}(x)$ [see Eq. (B13)]. Indeed, the transformation $\Phi_\pm\to\Phi_\pm+\Phi_{0,\pm}$ of the chiral boson fields gauges away bias term (6). We note that, differently from the homogenous Luttinger liquid case, in the presence of leads the zero modes cannot be just linear functions of the position uniformly along the entire system. The inhomogeneity of the system leads to a nontrivial space dependence of the zero modes $\Phi_{0,\pm}(x)$, which can be obtained from the boson Green's function of the inhomogeneous LL model, as shown in Eq. (B14).

B. Interaction effects on electron tunneling from the tip: The case of adiabatic contacts

We shall now consider the full three-terminal setup and discuss the effects of the wire electron-electron interaction on tunneling from the tip, both for the case of electron injection and in the voltage-probe configuration. We start by presenting results for a wire with adiabatic contacts ($\lambda_i=0$). For a noninteracting wire, the calculation described in Sec. III yields

$$I_T=\frac{e^2}{h}\frac{8\gamma^2}{(2+\gamma^2)^2}\left(V_T-\frac{1+\chi}{2}V_S-\frac{1-\chi}{2}V_D\right), \tag{54}$$

and

$$I_M=\frac{e^2}{h}\frac{1}{(2+\gamma^2)^2}\{V_S[4+2\gamma^2(1-\chi+\gamma^2\chi^2)] - V_D[4+2\gamma^2(1+\chi+\gamma^2\chi^2)]+4\chi\gamma^2V_T\}, \tag{55}$$

where γ is the total tunneling strength defined in Eq. (34) and χ is the tunneling asymmetry parameter introduced in Eq. (35). Thus, in the absence of interaction, the currents depend linearly on the three applied voltages and are independent of the position x_0 of the tip.

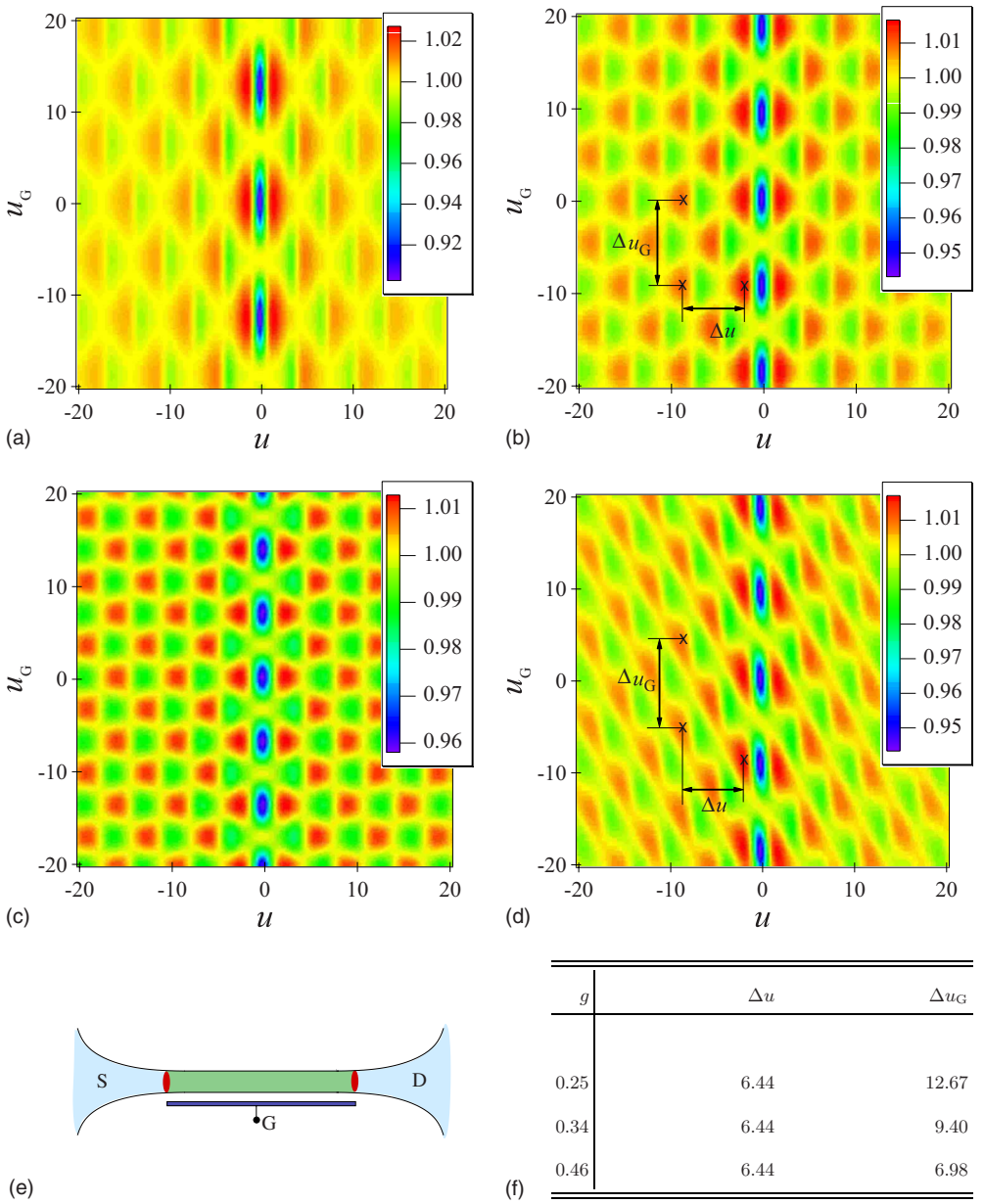

g	Δu	Δu_G
0.25	6.44	12.67
0.34	6.44	9.40
0.46	6.44	6.98

FIG. 6. (Color online) The differential conductance dI_M/dV [in units of $(e\omega_L^*/2\pi)$] of the two-terminal setup (in the absence of a tip) is shown as a function of the dimensionless source-drain bias u and the dimensionless gate voltage u_G. The strengths of the contact impurities are equal and are characterized by $\lambda_{F,i}=0.1$ and $\lambda_{B,i}^*=0.25$. In panels (a), (b), and (c) the source-drain voltage is applied symmetrically, $u_{S/D}=\pm u/2$, and the interaction parameter is $g=0.25$, 0.34, and 0.46, respectively. The dashed-dotted lines in panels (b) and (d) are a guide for the eyes to identify the periodic pattern of the Fabry-Pérot oscillations determined by the periods Δu and Δu_G. Their ratio yields the value of g, as shown in the table for the three cases. In panel (d) the source-drain voltage is applied asymmetrically ($u_S=u$ and $u_D=0$) to a wire with interaction strength $g=0.34$. When compared with panel (b) for the same interaction strength, the asymmetric bias twists the pattern.

When electron-electron interaction is taken into account, an exact solution of the tunneling problem is not possible for arbitrary values of the tunneling amplitudes $\gamma_\pm$. We shall assume that $\gamma_\pm \ll 1$, consistent with the tunnel Hamiltonian approach, and provide results to leading order in perturbation theory. The currents in the source and drain leads are again written as in Eqs. (16) and (17), where I_M and I_T are evaluated now to order γ^2 yielding

$$I_M = I_0 + I_{M,\gamma^2}, \tag{56}$$

and

$$I_T = I_{T,\gamma^2}, \tag{57}$$

where

$$I_{M(T),\gamma^2} = \frac{e\omega_L^*}{2\pi}(\gamma^*)^2 j_{M(T),\gamma^2}. \tag{58}$$

Here

$$\gamma^* = \gamma \alpha_W^{(g+g^{-1}-2)/4} \tag{59}$$

is the tunneling amplitude renormalized by the electron-electron interaction. The dimensionless currents $j_{M(T),\gamma^2}$ read as

$$j_{M(T),\gamma^2} = \frac{2}{\pi \alpha_T \alpha_W^{(g+g^{-1})/2}} \int_0^\infty d\tau Q_{M(T)}(\tau) \sin\{4\pi[\mathcal{I}^{\Phi_+\Phi_+}(\xi_0;\xi_0;\tau) + \mathcal{I}^{\varphi\varphi}(0;0;\tau)]\} e^{4\pi[\mathcal{R}_{reg}^{\Phi_+\Phi_+}(\xi_0;\xi_0;\tau)+\mathcal{R}_{reg}^{\varphi\varphi}(0;0;\tau)]}, \tag{60}$$

where

$$Q_M(\tau) = \sin(u\tau/2)\cos[(u_W - u_T)\tau] + \chi \cos(u\tau/2)\sin[(u_W - u_T)\tau],$$

$$Q_T(\tau) = 2\cos(u\tau/2)\sin[(u_W - u_T)\tau] + 2\chi \sin(u\tau/2)\cos[(u_W - u_T)\tau]. \tag{61}$$

Here α_T is a small dimensionless cut-off parameter for the tip defined in Appendix B. The functions $\mathcal{R}_{reg}^{\Phi_+\Phi_+}(\xi;\xi';\tau)$ and $\mathcal{I}^{\Phi_+\Phi_+}(\xi;\xi';\tau)$ are the real and imaginary parts of the auto-correlation function of the chiral wire field Φ_+ defined in Eqs. (C7) and (C8), respectively, while $\mathcal{R}_{reg}^{\varphi\varphi}(\xi;\xi';\tau)$ and $\mathcal{I}^{\varphi\varphi}(\xi;\xi';\tau)$ are the real and imaginary parts of the correlator of the tip field φ given in Eqs. (C11) and (C12). The integral [Eq. (60)] is a cut-off independent quantity.

We consider two parameter domains of the three-terminal setup corresponding to the cases where the tip operates as an electron injector and as voltage probe, respectively. In the electron injection case, source and drain are at the same electrochemical potential while a bias is applied to the tip. For this configuration the current noise was evaluated in Refs. 17 and 18. Here we shall explicitly evaluate the nonlinear tunneling conductances,

$$G_{ST} \doteq \left.\frac{\partial I_S}{\partial V_T}\right|_{V_S=V_D=0} \tag{62}$$

and

$$G_{DT} \doteq \left.\frac{\partial I_D}{\partial V_T}\right|_{V_S=V_D=0}. \tag{63}$$

Conventional Luttinger liquid theory, where the presence of the source and drain electrodes is neglected, predicts that an electron charge injected by tunneling, e.g., as a right mover into an interacting wire breaks up into separate charge pulses moving in opposite directions, namely, a fraction $(1+g)/2$ moving to the right and a fraction $(1-g)/2$ going to the left.[18,27,35–38] This effect originates from the coupling between the densities of right-moving and left-moving electrons, accounted for by the homogeneous LL Hamiltonian. As a consequence, one expects that when the tip injects electrons asymmetrically, e.g., only toward the drain electrode on the right ($\chi=1$), the electron-electron interaction would cause a part of the current to flow also to the source electrode on the left.

However, when the source and drain electrodes are explicitly taken into account, our results show that the above expectation is in fact wrong. Remarkably, using Eq. (60), one can indeed prove that for $V_S=V_D$ the equality

$$\mathcal{A}(\chi) = \left.\frac{|I_D| - |I_S|}{|I_D| + |I_S|}\right|_\chi \equiv \chi \tag{64}$$

holds, indicating that for a clean wire the current asymmetry is *independent* of the wire interaction strength g. In particular, for fully asymmetric tunneling ($\chi=1$), the whole current is injected into the drain electrode, just as in the noninteracting case. This unidirectional charge flow even in the presence of interaction arises from the phenomenon of Andreev-type reflections.[22,23] Even though charge fractionalization occurs in the bulk of the wire, the plasmonic excitations reaching an interface with the leads experience the mismatch of the interaction strengths in the wire and in the electrode and are thus partly reflected as an oppositely charged excitation. The sum of all reflected pulses at both interfaces restores the property that the whole current flows into the drain, like in the noninteracting wire. This behavior is in fact very similar to an effect occurring in a two-terminal setup, where the conductance of a wire adiabatically connected to electrodes is $G_{2t}=e^2/h$, independent of the interaction strength. Thus, for perfectly transmitting contacts, it is impossible to extract the interaction constant neither from the conductance of a two-terminal setup nor from the current asymmetry in three-terminal measurements.

Nevertheless, in a three-terminal setup signatures of interaction *do appear* in the behavior of the differential conductances G_{ST} and G_{DT} as a function of the tip-source and tip-drain biases. Figures 7(a) and 7(b) show G_{ST} and G_{DT} for the case of a tip located in the middle of a wire with interaction strength $g=0.25$. The various curves correspond to different values of the asymmetry parameter χ, which unbalances the amount of injected right vs left-moving electrons. The fully symmetric case ($\chi=0$) was discussed in Ref. 39. While for a noninteracting wire G_{ST} and G_{DT} are constant [as can easily be seen from Eqs. (54) and (55)], in the presence of interaction an oscillatory behavior arises. These oscillations are entirely due to the electron-electron interaction in the wire, which causes Andreev-type reflections even at adiabatic contacts. With increasing χ the conductance G_{ST} decreases until it vanishes for $\chi=1$, whereas the conductance G_{DT} increases up to the maximum value for the completely asymmetric case. The relation $G_{ST}=G_{DT}(1-\chi)/(1+\chi)$ between these two conductances is independent of g.

Figures 7(c) and 7(d) describe the case of an off-centered tip located at $x_0=0.45L$. Apparently, the period of the oscillations is the same as in panels (a) and (b) where the tip is in the middle. This is due to the fact that this period is related to the traversal time of plasmonic excitations originating from the tip and interfering at the same point after an even number of Andreev-type reflections at the contacts. This traversal time depends neither on x_0 nor on the asymmetry coefficient.

Let us now discuss the configuration where the tip acts as a voltage probe, i.e., when $V_S \neq V_D$ and V_T is set to a value such that $I_T=0$ is fulfilled. In this configuration the quantity on the left-hand side of Eq. (36) is vanishing due to Eqs. (16)

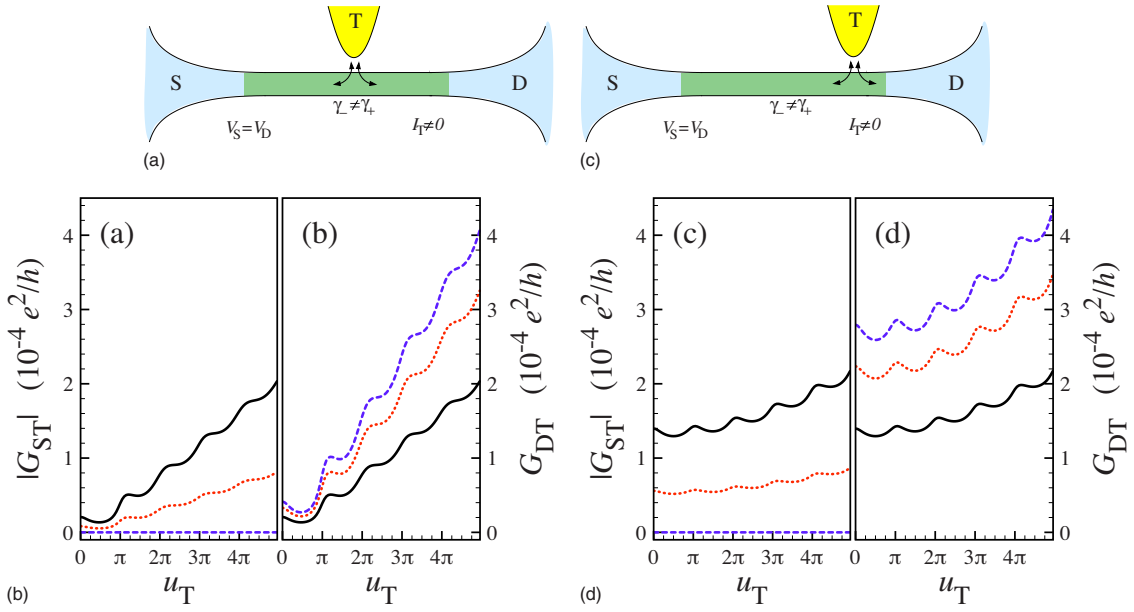

FIG. 7. (Color online) Electron injection into an interacting wire. Panel (a) [(b)] shows the tunneling differential conductance G_{TS} (G_{TD}) between the tip and source (drain) electrode as a function of the dimensionless tip-source (tip-drain) bias for a wire with interaction strength $g=0.25$. The various curves refer to different values of the tunneling asymmetry ($\chi=0$ solid line, $\chi=0.6$ dotted line, and $\chi=1$ dashed line). The tunneling strength is $\gamma^*=0.01$, and the tip is located in the middle of the wire. Panels (c) and (d) are the same as panels (a) and (b) but the tip is located near a contact at $x_0=0.45L$.

and (17). By applying a source-drain bias, one can analyze how the source-drain conductance,

$$G_{SD} = \left.\frac{\partial I_M}{\partial (V_S - V_D)}\right|_{I_T=0}, \tag{65}$$

is affected by the interaction strength. It is worth emphasizing that in a two-terminal setup, i.e., in the absence of the tip ($\gamma_\pm=0$), one obtains for a clean wire $G_{SD}=G_{2t}=e^2/h$, independent of the interaction strength. As already mentioned previously, this is due to the fact that, although the electron charge injected by the source splits up in fractions through the interaction-induced Andreev-type reflections at the contacts, in a clean wire the series of these fractions always sums up to e, disguising the interaction effects in the dc average current.[22] Our results show that a quite different behavior emerges for a three-terminal setup even in the configuration where the tip does not inject any net current into the wire. Figure 8(a) shows G_{SD} as a function of the source-drain bias, for different values of the interaction strength, ranging from a noninteracting to a strongly interacting wire. The left panel refers to the case of symmetric tunneling $\chi=0$, whereas the right one analyzes the role of a tunneling asymmetry. As one can see, the effects of interaction in the wire become observable through the voltage probe since oscillation of G_{SD} originating from Andreev-type reflections emerge. Notice that at constant bare tunneling amplitude γ the zero bias conductance is higher in the presence of interaction than for a noninteracting wire since the renormalization [Eq. (59)] of the tunneling amplitude suppresses γ. With increasing tunneling asymmetry [see Fig. 8(b)], the differences between interacting and noninteracting wires become less pronounced, and indeed the oscillations are washed out for fully asymmetric tunneling $\chi=\pm 1$.

The dimensionless tip voltage $\bar{u}_T=(e/\hbar\omega_L^*)\bar{V}_T$ ensuring $I_T=0$ shows an interesting dependence on the source-drain bias. In the limiting cases of symmetric and completely asymmetric tunneling this dependence coincides for interacting and noninteracting wires (namely, $\bar{u}_T=u_W$ for $\chi=0$ and $\bar{u}_T=u_W \pm u/2$ for $\chi=\pm 1$). For intermediate values of the asymmetry parameter χ the tip voltage $\bar{u}_T$ shows an oscillatory behavior with period $\Delta\bar{u}_T=2\pi$ as a function of the source-drain bias. We also see that the period of G_{SD} in Fig. 8 is twice as large as the period of G_{TS} and G_{TD} in Fig. 7 where the tip is in the electron injection configuration. This is due to the fact that in Fig. 8 the source-drain bias is applied symmetrically ($u_W=0$), while in Fig. 7 source and drain are both grounded and the bias is only applied to the tip.

Finally, we emphasize again the difference between the electron injection and the voltage-probe configurations of the tip: While in the former case an asymmetry in tunneling does not spoil the observation of effects of electron-electron interaction (see Fig. 7), in the latter case interaction-induced oscillations can be best observed for symmetric tunneling, and they are in fact vanishing for fully asymmetric tunneling.

C. Interaction effects on electron tunneling from the tip: The case of a wire with nonideal contacts

In this section we analyze the three-terminal transport properties in the presence of electron-electron interaction, contact impurity scattering, and electron tunneling from the tip. In particular, we discuss how a finite contact resistance modifies the Andreev-type oscillations of the tunneling conductances, previously discussed for the case of adiabatic con-

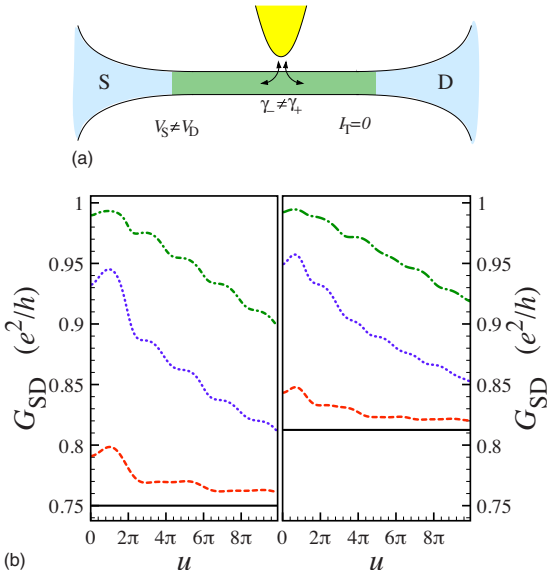

FIG. 8. (Color online) The effect of the tip in the voltage-probe configuration on the zero-temperature conductance is shown as a function of the source-drain bias. Panel (a) the case of symmetric tunneling ($\chi=0$). Panel (b) the case of an asymmetry in tunneling ($\chi=1/2$). Different curves refer to different values of the interacting strength: noninteracting ($g=1$, solid curve), weakly interacting ($g=0.7$, dashed curve), moderately interacting ($g=0.4$, dotted curve), and strongly interacting ($g=0.25$, dashed-dotted curve). The bare tunneling strength is $\gamma=0.5$ and the dimensionless cut-off parameter is $\alpha_W=10^{-3}$.

tacts ($\lambda_i=0$). We present results obtained by perturbation theory for weak contact impurities λ_i and tunneling amplitudes $\gamma_\pm$. Technical details can be found in Appendixes A and C. The currents may be written as

$$I_M = I_0 + I_{imp} + I_{M,\gamma^2} + I_{M,\gamma^2\lambda}, \tag{66}$$

and

$$I_T = I_{T,\gamma^2} + I_{T,\gamma^2\lambda}. \tag{67}$$

Here $I_0=(e^2/h)(V_S-V_D)$ is the current of an ideally contacted wire in the absence of the tip, whereas I_{imp} is the leading-order term accounting for nonideal contacts [see Eq. (45)]. In general, this latter term involves both Fabry-Pérot and Andreev-type oscillations. Both, I_0 and I_{imp}, vanish when the electrochemical potentials for source and drain electrodes are equal ($V_S=V_D$); alternatively, they can be easily determined by measuring the current-voltage characteristics in the absence of the tip. Henceforth, we shall focus on contributions to the currents arising from the presence of the tip. The leading-order terms I_{M,γ^2} and I_{T,γ^2}, given by Eq. (58), describe tunneling into an ideally contacted wire and contain only Andreev-type oscillations. The next-to-leading-order terms ($\gamma^2\lambda,\gamma^2\lambda^2,\ldots$) also exhibit oscillations originating from interference between backscattering at the contacts and tunneling to or from the tip. Such oscillations although modified by the interaction are already present in a noninteracting wire, unlike the Andreev-type oscillations of the leading-order terms (γ^2) that are instead entirely due to the interaction. We thus analyze how interaction affects the terms $I_{T(M),\gamma^2\lambda}$, which represent the most relevant correction to the Andreev-type oscillations discussed above. These terms describe to leading order the interplay between electron injection at the tip and backscattering at the S and D contacts.

Explicitly one finds

$$I_{M(T),\gamma^2\lambda} = \frac{e\omega_L^*}{2\pi}(\gamma^*)^2\lambda^*\sqrt{1-\chi^2}\, j_{M(T),\gamma^2\lambda}, \tag{68}$$

where $\lambda^*=\lambda^*_{B,1}+\lambda^*_{B,2}$, and

$$j_{M(T),\gamma^2\lambda} = -\frac{1}{2\pi\alpha_W^{(g+g^{-1}+6)/4}\alpha_T}\sum_{i=1,2}\frac{\lambda^*_{B,i}}{\lambda^*}\int\int_{-\infty}^{+\infty} d\tau_1 d\tau_2 \Big(\cos[(u_S-u_T)\tau_1+(u_T-u_D)\tau_2-2(\kappa_W+gu_W-gu_G)(\xi_0-\xi_i)]$$
$$\times e^{4\pi[\mathcal{R}_W(\xi_0;\xi_i;\tau_1;\tau_2)+\mathcal{R}_T(\tau_1;\tau_2)]}\sum_{\eta_1,\eta_2=\pm} P^{\eta_1\eta_2}_{M(T)}F^{\eta_1\eta_2}_{W,\gamma^2\lambda}(\tau_1;\tau_2)F^{\eta_1\eta_2}_{T,\gamma^2\lambda}(\tau_1;\tau_2)\sin\{4\pi[\mathcal{I}^{\eta_1}_W{}^{\eta_2+}(\xi_0;\xi_i;\tau_1;\tau_2)+\mathcal{I}^{\eta_1\eta_2}_T(\tau_1;\tau_2)]\}\Big), \tag{69}$$

where

$$P^{\eta_1\eta_2}_M = \eta_2+\eta_1-2\eta_1\eta_2, \tag{70}$$

$$P^{\eta_1\eta_2}_T = 2(\eta_2-\eta_1). \tag{71}$$

The functions $F^{\eta_1\eta_2\eta_3}_{W,\gamma^2\lambda}(\tau_1;\tau_2)$ and $F^{\eta_1\eta_2}_{T,\gamma^2\lambda}(\tau_1;\tau_2)$ are defined in Appendix B in Eqs. (B8) and (B24), respectively, and the functions $\mathcal{R}_W(\xi_0;\xi_i;\tau_1;\tau_2)$, $\mathcal{I}_W(\xi_0;\xi_i;\tau_1;\tau_2)$, $\mathcal{R}_T(\tau_1;\tau_2)$, and $\mathcal{I}_T(\tau_1;\tau_2)$, accounting for the real and the imaginary parts of several correlation functions in the wire and in the tip, are defined in Appendix C in Eqs. (C1), (C2), (C11), and (C12), respectively.

For simplicity, we limit the analysis of Eqs. (68) and (69) to the electron injection configuration where source and drain are grounded. We start with the case of symmetric tunneling ($\chi=0$).

As already observed in Sec. III for a noninteracting wire, term (68) leads to additional oscillations in the differential conductance of the three-terminal setup. These conventional oscillations are characterized by two periods related to the

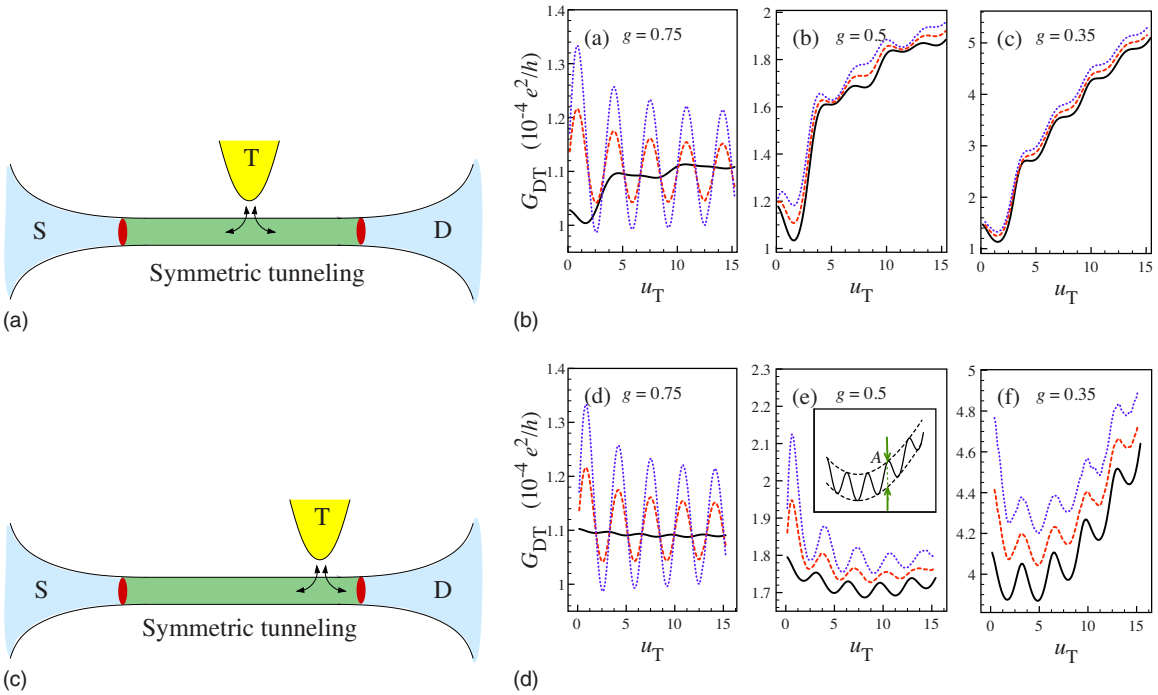

FIG. 9. (Color online) Zero-temperature nonlinear tip-drain conductance G_{DT} as a function of the tip bias for tunneling amplitude $\gamma^* = 10^{-2}$ and symmetric tunneling $\chi=0$. The upper panels (a), (b), and (c) are related to a tip in the middle of the wire ($x_0=0$), whereas the lower ones (d), (e), and (f) to a tip located at $x_0=0.45L$. Panels pairs (a) and (d), (b) and (e), and (c) and (f) describe the case of a wire with weak ($g=0.75$), moderate ($g=0.5$), and strong ($g=0.35$) interaction strength, respectively. In each panel the different curves refer to different contact impurity strengths. The solid curves describe the case of ideal contacts where the oscillations are purely Andreev type. The dashed (dotted) lines refer to finite contact impurity strength $\lambda^*_{B,1}=\lambda^*_{B,2}=0.1$ (=0.2). For a weakly interacting wire the conductance oscillations are mostly due to the conventional interference between backscattering at the contacts and tip tunneling and Andreev-type oscillations become visible only for extremely low contact resistance. In contrast, for stronger interaction strength a finite contact resistance is sufficient for the oscillations to be attributed to Andreev-type processes. The inset of panel (e) shows the definition of the average amplitude referred to in the text.

distances between the tip and the contact impurities so that the pattern depends on the tip position. Electron-electron interaction modifies this pattern reducing the amplitude of the conventional oscillations and giving rise to additional Andreev-type oscillations. The case of a tip in the middle of the wire is shown in the upper panels (a), (b), and (c) of Fig. 9, where the differential conductance G_{DT} is plotted as a function of the tip bias u_T for three different values of interaction strength, ranging from weak ($g=0.75$), over moderate ($g=0.5$) to strong interaction ($g=0.35$), as displayed in the three panels. In each panel the solid curve refers to the case of ideal contacts where the oscillations are purely of Andreev type. The dotted and dashed curves describe the effect of finite contact resistances arising from the contribution of term (68). As one can see from panel (a), for weak electron-electron interaction the conventional oscillations dominate and mask the Andreev-type oscillations. In this case, only extremely good contacting might allow one to identify Andreev-type processes. However, for moderate interaction strength [panel (b)], the two types of oscillations have comparable amplitudes, and for strong interaction [panel (c)] the conventional oscillations are strongly suppressed while term (68) only causes a small shift of the conductance value. The oscillations of G_{DT} are essentially Andreev type.

A similar effects occurs when the tip is closer to one of the contacts displayed in lower panels (d), (e), and (f) of Fig. 9. The main difference is that in this case the pattern of the Andreev-type oscillations is more sinusoidal even for weak interactions.

Our result indicates that, for a wire with a given interaction strength, there is crossover value λ^*_C of the (renormalized) contact resistance, below which the oscillations of the nonlinear conductance can essentially be attributed to Andreev-type processes. We have quantified λ^*_C for the case of a tip close to the contacts, where the regularity of oscillations allows for a straightforward determination of their amplitude, defined as the average distance between maxima and minima, as schematically displayed in the inset of Fig. 9(e). The crossover impurity strength λ^*_C is then simply determined by the value of λ^* for which the amplitude $A_{\gamma^2\lambda}$ of the conventional oscillation term $I_{T,\gamma^2\lambda}$ [see Eq. (68)] equals the amplitude A_{γ^2} of the Andreev-type oscillation term I_{T,γ^2} [see Eq. (58)]. The result is given in Table I for different values of interaction strength. For contact impurity strength $\lambda^* \leq \lambda^*_C$ the oscillations of the nonlinear conductance are essentially of Andreev type.

Let us finally briefly consider the case of asymmetric tunneling $\chi \neq 0$. An important result is that, in view of Eq. (68), the contribution to the current of order $\gamma^2\lambda$ vanishes in the case of totally asymmetric tunneling ($\chi = \pm 1$). This property is thus robust to electron-electron interaction within the Luttinger liquid picture. In fact, one can show that in this case

TABLE I. Crossover value of the (renormalized) contact impurity strength λ_C^*, below which oscillations can be attributed to Andreev-type processes, for various values of the interaction strength g. The tip is located at $x_0=0.45L$, like in the lower panels of Fig. 9.

g	0.4	0.5	0.6	0.7	0.8
λ_C^*	0.2	0.02	4×10^{-3}	4×10^{-4}	10^{-4}

only perturbative contributions of order $\gamma_i^{2n}(\lambda_1\lambda_2)^{n+m}$ ($n=1,2,3,\ldots;m=0,1,2,\ldots$) are nonvanishing.

V. DISCUSSION AND CONCLUSIONS

In the present work, we have investigated transport properties of a quantum wire contacted to source and drain reservoirs in the presence of a third electrode (tip) injecting electrons into the wire. We have tailored our model to account for various aspects of a typical experimental situation by including finite contact resistances and the presence of a gate in addition to electron-electron interaction and by analyzing the effect of the position of the tip as well as the role of a tunneling asymmetry. Specifically, we have considered both the situation where the tip behaves as an electron injector and the voltage-probe configuration. We have found that the three-terminal setup exhibits extremely rich behaviors, determined not only by each of the above aspects but also by their interplay. In order to facilitate the discussion, we propose to the reader different perspectives from which our results can be considered.

The effects of electron-electron interaction on Fabry-Pérot oscillations. The origin of Fabry-Pérot oscillations boils down to quantum interference between electron backscattering at two (or more) impurities. As a consequence, this phenomenon is present also in a noninteracting quantum wire (see Sec. III), where the oscillations appear both as a function of the source-drain bias and as a function of the gate voltage. The interference pattern is modified by electron-electron interaction, which introduces a power-law suppression of the amplitude and, especially for $g<1/2$, deforms the sinusoidal shape toward a sawtoothlike shape (see Fig. 5). Interaction also leads to a (partial) screening of the charge in the wire,[34] causing a change in the oscillation period as a function of the gate bias with respect to the period as a function of the source-drain bias. This effect suggests an operative procedure to extract the Luttinger liquid parameter g from measurements of the nonlinear conductance in the Fabry-Pérot regime (see Fig. 6). The effects of an asymmetrically applied source-drain bias have also been discussed. We emphasize that, differently from previous approaches adopted in the literature, our way to introduce the biasing voltages correctly recovers both gauge invariance[28] and the property that, in the limit of strong interaction $g\to0$, the current-voltage characteristics only depends on the difference between source and drain biases V_S-V_D.

Conventional vs Andreev-type oscillations. Besides modifying Fabry-Pérot oscillations, electron-electron interaction also yields another major effect, which is absent in a noninteracting wire: At the wire-electrode interfaces, plasmon excitations are partially reflected due to the mismatch of interaction strengths in the interacting wire and the noninteracting electrodes. This effect, entirely due to interaction, occurs also for ideally contacted adiabatic interfaces and gives rise to a different type of oscillations, which are termed Andreev-type oscillations[32] since the incoming charge and the fractional charge reflected at the contact have opposite signs, just as at an interface between a normal metal and a superconductor. In real experiments with interacting quantum wires in the Fabry-Pérot regime, the current-voltage characteristics will in general exhibit both conventional Fabry-Pérot oscillations, i.e., oscillations that are already present in a noninteracting wire and that are simply *modified* by interaction, and Andreev-type oscillations, purely *originating* from interaction. The interesting question arises whether one can distinguish between these two oscillatory phenomena in an operative way and, in particular, whether it is possible to determine regimes and conditions, under which the latter can be observed.

Since the amplitude of Fabry-Pérot oscillations is roughly proportional to the reflection coefficients of the contacts, whereas Andreev-type processes occur even with ideal interfaces, one might at first think that with improving transparency of the contacts the nonlinear conductance of a two-terminal setup would exhibit a predominance of Andreev-type oscillations over the conventional Fabry-Pérot ones. This is, however, not the case, since for an ideally contacted wire the sum of all Andreev-type reflection processes at the two interfaces exactly recovers the injected pulse when the sign of all reflected charge pulses is taken into account. The transmission of an interacting wire adiabatically connected to noninteracting leads turns out to equal 1, as was pointed out in Refs. 22 and 23. Although Andreev-type oscillations of the conductance do appear in the presence of even a single impurity,[32] their amplitude is proportional to the impurity reflection coefficient. This implies that two-terminal setups are not suitable to distinguish between Andreev-type and Fabry-Pérot oscillations since both oscillations have the same dependence on the impurity strengths $\lambda_{B,i}^*$. Furthermore they also exhibit the same period as a function of the source-drain bias.

In contrast, our analysis suggests that a three-terminal setup may allow one to distinguish Andreev-type oscillations from conventional oscillations. As far as Andreev-type oscillations are concerned, three-terminal setups indeed offer one important advantage with respect to two-terminal ones: in the presence of a third electrode, Andreev-type oscillations appear even for the ideal case of a wire adiabatically connected to the source and drain electrodes ($\lambda_i=0$). In the presence of interaction the tip-source and tip-drain nonlinear conductances G_{ST} and G_{DT} oscillate as a function of the tip voltage u_T already to leading order γ^2 in the tunneling amplitude, independent of contact impurity strengths λ_i. This effects holds when the tip acts as an electron injector (see Fig. 7) as well as when it acts as a voltage probe (see Fig. 8), and the oscillations vanish for a noninteracting wire [see Eqs. (54) and (55)]. Thus, quite differently from a two-terminal setup, in three-terminal setups Andreev-type oscillations become better visible when the contact transparency is improved.

In view of the fact that in realistic experiments the contact resistance is always finite, we have quantitatively evaluated the influence of the contact resistance on the conductance oscillations [see Eq. (69)] showing that additional Fabry-Pérot-type oscillations superimpose with the Andreev-type ones (see Fig. 9). We have thus put forward criteria for observing the interaction induced Andreev-type oscillations. At least two experimental situations are promising: For the conventional case of symmetric tunneling form the tip, we have determined typical values of the contact resistance below which the oscillations in the current-voltage characteristics can essentially be attributed to Andreev-type phenomena. The result, shown in Table I, indicates that the stronger the interaction of the wire the larger are the contact resistances that are tolerable to still observe Andreev-type oscillations. Furthermore, in case that the setup allows for fully asymmetric tunneling, the leading-order correction (69) competing with the Andreev-type term is vanishing even in the presence of interaction.

In summary, in systems such as carbon nanotubes where the interaction strength is typically strong, $g \simeq 0.2-0.3$, while electron injection from an STM tip is typically symmetric, Andreev-type oscillations may be observed by achieving a high quality of the contacts to the leads. In contrast, in semiconductor quantum wires, where the interaction strength is usually moderate $g \simeq 0.6-0.7$, asymmetric tunneling induced by a magnetic field is more suitable to observe Andreev-type oscillations.

The effects of asymmetric tunneling. The above-mentioned case of asymmetric tunneling deserves some further remarks. Recent experiments by Yacoby and co-workers[12,21] showed that fully asymmetric tunneling into semiconductor-based quantum wires can be realized by appropriate tuning of a magnetic field. Inspired by these experiments, we have considered the possibility of an asymmetry in electron tunneling from the tip. Before discussing our results we would like to point out the relation between our model and Yacoby's experimental setup. While Yacoby *et al.*[8] studied electron tunneling between two parallel wires where momentum conservation is required, our model considers injection from a pointlike tip. Although these two situations may at first seem incompatible, a regime can be determined where they are equivalent. In the experiments of Refs. 12 and 21 electrons are injected from an upper shorter wire with length L_u into a lower longer wire with length L_l. Since the tunneling region reasonably coincides with the length of the short wire, momentum conservation only holds up to an uncertainty $\delta k \sim 1/L_u$. Although this uncertainty is small enough to select a specific electron momentum state in the upper wire, δk may be much bigger than the mean level spacing of the lower wire if the latter is much longer than the former ($L_l \gg L_u$). In this regime, while the electron wave function behaves like a plane wave for the short wire, for the long wire it can effectively be considered as a localized wave packet, and our model applies.

Under these conditions several interesting effects emerge. In the first instance, by using the tip as an electron injector, the tunneling asymmetry can be exploited to gain the transmission coefficient of each contact by measuring the current asymmetry [Eq. (36)] in the two cases of tunneling purely to the right ($\chi=+1$) and to the left ($\chi=-1$), as has been shown in Eq. (40). Second, when the tip is used in the configuration of a voltage probe, fully asymmetric tunneling allows one to eliminate the suppression of the source-drain conductance G_{SD}, which occurs for symmetric tunneling. Similarly, G_{SD} becomes independent of the tip position.

When electron-electron interaction is taken into account, the scenario is even richer. Luttinger liquid theory predicts that electron-electron interaction induces a current asymmetry which depends on the interaction strength g. The appealing question arises whether this effect is observable in experiments, where currents are measured not directly in the interacting wire but in metallic electrodes connected to it. The investigation carried out in Ref. 27, based on the assumption that the interfaces between the interacting wire and the electrodes can be treated phenomenologically with a transmission coefficient *à la* Landauer-Büttiker, has led these authors to the claim that the interaction strength can be observed via the current asymmetry. Here we have scrutinized this prediction by taking the presence of source and drain electrodes into account fully consistently within the inhomogeneous Luttinger liquid model. Considering as a test bench the case of a wire adiabatically contacted to source and drain electrodes, we have proven that, although charge fractionalization does occur in the bulk of the wire, the sum of Andreev-type reflection processes at the contacts leads to a current asymmetry $\mathcal{A}$ that is independent of the electron-electron interaction strength, just as it is the case with the two terminal conductance G_{2t}. Thus, already for this ideal case, no proof of charge fractionalization can be gained from the analysis of $\mathcal{A}$ or from the ration $e^2\mathcal{A}/(hG_{2t})$. We have also shown that, nevertheless, interaction effects do appear in the behavior of the nonlinear conductance where interaction induced oscillations arise as a function of the tip-source and tip-drain biases. It is worth emphasizing that this feature is due to the three-terminal setup since the two-terminal conductance of a Luttinger liquid ideally contacted to leads is independent of the source-drain bias.

ACKNOWLEDGMENTS

The authors acknowledge stimulating discussions with R. Fazio, T. Martin, P. Recher, and B. Trauzettel, and computational support by D. Passerone. Funding was provided by the Deutsche Forschungsgemeinschaft (DFG), by the NANOFRIDGE EU Project, by the Rientro dei Cervelli MIUR Program, as well as by the Italian-German collaboration program Vigoni.

APPENDIX A: KELDYSH FORMALISM AND PERTURBATIVE EVALUATION OF THE CURRENT

In order to compute the current in the three terminal setup, we adopt the Keldysh formalism[30] suitable to account for out-of-equilibrium properties. According to Eq. (14), the current at position x (located in the source or in drain leads) and time t can be written as

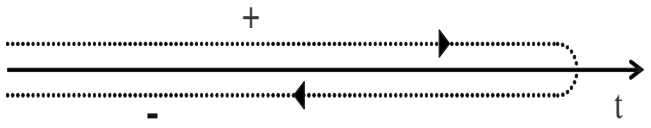

FIG. 10. Keldysh contour along the time axis.

$$I(x,t) = \frac{ev_{\mathrm{W}}}{2} \sum_{\eta=\pm} \langle j^{(\eta)}(x,t) \rangle, \tag{A1}$$

where

$$j^{(\eta)}(x,t) = \sum_{r=\pm} r{:}\Psi_r^{\dagger(\eta)}(x,t)\Psi_r^{(\eta)}(x,t){:}. \tag{A2}$$

Here $\eta=+$ $(\eta=-)$ corresponds to the upper (lower) branch of the Keldysh contour depicted in Fig. 10. The current $I(x,t)$ and various other quantities introduced below also depend on the injection point x_0 and the impurity positions x_1 and x_2. These variables will frequently be suppressed to simplify notation.

In the Keldysh interaction picture with

$$\mathcal{H}_0 = \mathcal{H}_{\mathrm{kin,W}} + \mathcal{H}_U + \mathcal{H}_{\mathrm{kin,T}} \tag{A3}$$

and

$$\mathcal{H}_{\mathrm{I}} = \mathcal{H}_\lambda + \mathcal{H}_{\mathrm{tun}} + \mathcal{H}_{\mu_{\mathrm{W}}} + \mathcal{H}_{\mu_{\mathrm{T}}}, \tag{A4}$$

one obtains

$$I(x,t) = \frac{ev_{\mathrm{W}}}{2} \sum_{\eta=\pm} \left\langle T_{\mathrm{K}} \left[j^{(\eta)}(x,t) \times \exp\left(-i/\hbar \sum_{\eta'=\pm} \eta' \int_{-\infty}^{\infty} dt' \mathcal{H}_{\mathrm{I}}^{(\eta')}(t') \right) \right] \right\rangle_0, \tag{A5}$$

where $\langle \ldots \rangle_0$ denotes the average with respect to the equilibrium state determined by the Hamiltonian $\mathcal{H}_0$ and T_{K} is the Keldysh time-ordering operator. Expanding the exponent in Eq. (A5) perturbatively in terms of γ and λ, one obtains the current to the desired order. Below we sketch the calculation of $I_{\gamma^2\lambda}$, i.e., the contribution of order $\gamma^2\lambda$ to $I(x,t)$. With the abbreviations

$$\mathcal{U}_{\mathrm{W}} = \exp\left(-\frac{i}{\hbar} \sum_{\eta'=\pm} \eta' \int_{-\infty}^{\infty} dt' \mathcal{H}_{\mu_{\mathrm{W}}}^{(\eta')}(t') \right),$$

$$\mathcal{U}_{\mathrm{T}} = \exp\left(-\frac{i}{\hbar} \sum_{\eta'=\pm} \eta' \int_{-\infty}^{\infty} dt' \mathcal{H}_{\mu_{\mathrm{T}}}^{(\eta')}(t') \right), \tag{A6}$$

one obtains[40]

$$\begin{aligned} I_{\gamma^2\lambda}(x,t) &= \frac{iev_{\mathrm{W}}^3 v_{\mathrm{T}}}{4} \sum_{i=1,2} \sum_{r_1,r_2=\pm} \lambda_i \gamma_{r_1} \gamma_{r_2} \int\int\int dt_1 dt_2 dt_3 \sum_{\eta,\eta_1,\eta_2,\eta_3=\pm} \eta_1\eta_2\eta_3 \\ &\times \Bigg\langle T_K \Bigg\{ j^{(\eta)}(x,t) \mathcal{U}_{\mathrm{W}} \mathcal{U}_{\mathrm{T}} [e^{-i(r_1-r_2)k_{\mathrm{W}}x_0} \Psi_{r_1}^{\dagger(\eta_1)}(x_0,t_1) c^{(\eta_1)}(0,t_1) c^{\dagger(\eta_2)}(0,t_2) \Psi_{r_2}^{(\eta_2)}(x_0,t_2) + e^{i(r_1-r_2)k_{\mathrm{W}}x_0} c^{\dagger(\eta_1)}(0,t_1) \\ &\times \Psi_{r_1}^{(\eta_1)}(x_0,t_1) \Psi_{r_2}^{\dagger(\eta_2)}(x_0,t_2) c^{(\eta_2)}(0,t_2)] \sum_{r_3=\pm} e^{-2ir_3k_{\mathrm{W}}x_i} \Psi_{r_3}^{\dagger(\eta_3)}(x_i,t_3) \Psi_{-r_3}^{(\eta_3)}(x_i,t_3) \Bigg\} \Bigg\rangle_0 \\ &= -\frac{ev_{\mathrm{W}}^3 v_{\mathrm{T}}}{2} \sum_{i=1,2} \sum_{r_1,r_2=\pm} \lambda_i \gamma_{r_1} \gamma_{r_2} \int\int\int dt_1 dt_2 dt_3 \sum_{\eta,\eta_1,\eta_2,\eta_3=\pm} \eta_1\eta_2\eta_3 \Im \Bigg\langle T_K \Bigg\{ j^{(\eta)}(x,t) \mathcal{U}_{\mathrm{W}} \mathcal{U}_{\mathrm{T}} [e^{-i(r_1-r_2)k_{\mathrm{W}}x_0} \Psi_{r_1}^{\dagger(\eta_1)}(x_0,t_1) \\ &\times c^{(\eta_1)}(0,t_1) c^{\dagger(\eta_2)}(0,t_2) \Psi_{r_2}^{(\eta_2)}(x_0,t_2)] \sum_{r_3=\pm} e^{-2ir_3k_{\mathrm{W}}x_i} \Psi_{r_3}^{\dagger(\eta_3)}(x_i,t_3) \Psi_{-r_3}^{(\eta_3)}(x_i,t_3) \Bigg\} \Bigg\rangle_0, \end{aligned} \tag{A7}$$

where we have used the properties,

$$\langle T_K [A^{(\eta_A)}(t_A) B^{(\eta_B)}(t_B) \ldots Z^{(\eta_Z)}(t_Z)] \rangle^* = \langle T_K [Z^{\dagger(-\eta_Z)}(t_Z) \ldots B^{\dagger(-\eta_B)}(t_B) A^{\dagger(-\eta_A)}(t_A)] \rangle \tag{A8}$$

and

$$\mathcal{U}_{\mathrm{W,T}} = \left[\exp\left(-\frac{i}{\hbar} \sum_{\eta'=\pm} \eta' \int_{-\infty}^{\infty} dt' \mathcal{H}_{\mu_{\mathrm{W,T}}}^{(-\eta')}(t') \right) \right]^\dagger. \tag{A9}$$

Since the electron-electron interaction [Eq. (8)] contains only forward-scattering terms, all nonvanishing wire correlation functions must involve an even number of operators with a given chirality r. This yields $r_2=-r_1=r_3$ so that

$$\begin{aligned} I_{\gamma^2\lambda}(x,t) = &-\frac{ev_{\mathrm{W}}^3 v_{\mathrm{T}}}{2} \gamma_+ \gamma_- \sum_{i=1,2} \lambda_i \int\int\int dt_1 dt_2 dt_3 \sum_{\eta,\eta_1,\eta_2,\eta_3=\pm} \eta_1\eta_2\eta_3 \\ &\times \sum_{r_3=\pm} \Im \{ e^{2ir_3k_{\mathrm{W}}(x_0-x_i)} \langle T_K [j^{(\eta)}(x,t) \mathcal{U}_{\mathrm{W}} \mathcal{U}_{\mathrm{T}} \Psi_{-r_3}^{\dagger(\eta_1)}(x_0,t_1) c^{(\eta_1)}(0,t_1) c^{\dagger(\eta_2)}(0,t_2) \Psi_{r_3}^{(\eta_2)}(x_0,t_2) \Psi_{r_3}^{\dagger(\eta_3)}(x_i,t_3) \Psi_{-r_3}^{(\eta_3)}(x_i,t_3)] \rangle_0 \}. \end{aligned} \tag{A10}$$

The term with $r_3=+$ can be shown to yield the same contribution as the term with $r_3=-$. To see this explicitly, one makes use of $\mathfrak{I}(z)=-\mathfrak{I}(z^*)$, exploits Eqs. (A8) and (A9), and renames variables according to $\eta\to-\eta$, $\eta_i\to-\eta_i$ $(i=1,2,3)$, and $t_1\leftrightarrow t_2$. One can then write

$$I_{\gamma^2\lambda}(x,t) = -ev_{\mathrm{W}}^3 v_{\mathrm{T}}\gamma_+\gamma_-\sum_{i=1,2}\lambda_i\int\int\int dt_1dt_2dt_3\sum_{\eta_1,\eta_2,\eta_3=\pm}\eta_1\eta_2\eta_3\mathfrak{I}\{e^{-2ik_W(x_0-x_i)}\mathrm{W}_{\gamma^2\lambda,i}^{\eta_1\eta_2\eta_3}(t_1,t_2,t_3)\mathrm{T}_{\gamma^2}^{\eta_1\eta_2}(t_1,t_2)\}, \tag{A11}$$

where

$$\mathrm{W}_{\gamma^2\lambda,i}^{\eta_1\eta_2\eta_3}(t_1,t_2,t_3) = \sum_{\eta=\pm}\langle T_K[j^{(\eta)}(x,t)\mathcal{U}_{\mathrm{W}}\Psi_+^{\dagger(\eta_1)}(x_0,t_1)\Psi_-^{(\eta_2)}(x_0,t_2)\Psi_-^{\dagger(\eta_3)}(x_i,t_3)\Psi_+^{(\eta_3)}(x_i,t_3)]\rangle_0 \tag{A12}$$

contains correlation functions of wire operators, while

$$\mathrm{T}_{\gamma^2}^{\eta_1\eta_2}(t_1,t_2) = \langle T_K[\mathcal{U}_{\mathrm{T}}c^{(\eta_1)}(t_1)c^{\dagger(\eta_2)}(t_2)]\rangle_0 \tag{A13}$$

is a correlation function of the tip. These correlation functions are evaluated in Appendix B starting with Eq. (B7) and (B23), respectively. Inserting these results, one obtains

$$\begin{aligned}
I_{\gamma^2\lambda}(x,t) = {} & 2ev_{\mathrm{W}}\left(\frac{v_{\mathrm{W}}}{2\pi a_{\mathrm{W}}}\right)^2\frac{v_{\mathrm{T}}}{2\pi a_{\mathrm{T}}}\gamma_+\gamma_-\sum_{i=1,2}\lambda_i\int\int\int dt_1dt_2dt_3 \\
& \times\Re\Bigg\{e^{ie[(V_{\mathrm{S}}+V_{\mathrm{D}}-2V_{\mathrm{T}})(t_1-t_2)+(V_{\mathrm{S}}-V_{\mathrm{D}})(t_1-t_3+t_2-t_3)]/2\hbar}e^{-2i[k_{\mathrm{W}}+g^2e(V_{\mathrm{S}}+V_{\mathrm{D}}-2V_{\mathrm{G}})/\hbar v_{\mathrm{W}}](x_0-x_i)} \\
& \times\sum_{\eta_1,\eta_2,\eta_3=\pm}\eta_1\eta_2\eta_3F_{\mathrm{W}}^{\eta_1\eta_2\eta_3}(t_1-t_2,t_2-t_3)F_{\mathrm{T}}^{\eta_1\eta_2}(t_1-t_2)b_{\mathrm{W},\gamma^2\lambda,i}^{\eta_1\eta_2\eta_3}(t_1-t_3,t_2-t_3)b_{\mathrm{T},\gamma^2}^{\eta_1\eta_2}(t_1-t_2) \\
& \times\Bigg[\langle\partial_x\Theta(x,t)\Phi_+(x_0,t_1)\rangle_0^{\mathrm{Kel}}+\eta_1\langle\partial_x\Theta(x,t)\Phi_+(x_0,t_1)\rangle_0^{\mathrm{ret}}+\langle\partial_x\Theta(x,t)\Phi_-(x_0,t_2)\rangle_0^{\mathrm{Kel}}+\eta_2\langle\partial_x\Theta(x,t)\Phi_-(x_0,t_2)\rangle_0^{\mathrm{ret}} \\
& -\langle\partial_x\Theta(x,t)\Phi(x_i,t_3)\rangle_0^{\mathrm{Kel}}-\eta_3\langle\partial_x\Theta(x,t)\Phi(x_i,t_2)\rangle_0^{\mathrm{ret}}+\frac{1}{\pi\hbar}\int\int dx'dt'\mu_{\mathrm{W}}(x')\langle T_K[\partial_x\Theta(x,t)\partial_{x'}\Phi(x',t')]\rangle_0^{\mathrm{ret}}\Bigg]\Bigg\},
\end{aligned} \tag{A14}$$

where, for any pair of bosonic operators A and B, the following definitions hold

$$\langle A(t_A)B(t_B)\rangle^{\mathrm{Kel}} = \langle\{A(t_A),B(t_B)\}\rangle, \tag{A15}$$

$$\langle A(t_A)B(t_B)\rangle^{\mathrm{ret}} = \theta(t_A-t_B)\langle[A(t_A),B(t_B)]\rangle, \tag{A16}$$

$$\langle A(t_A)B(t_B)\rangle^{\mathrm{adv}} = -\theta(t_B-t_A)\langle[A(t_A),B(t_B)]\rangle. \tag{A17}$$

We now observe that the last term in Eq. (A14) can be dropped. Indeed, since it depends neither on η_i nor on t_i $(i=1,2,3)$, it can be singled out of the sums Σ_{η_i} and integrals $\int dt_i$; the remaining sums and integrations yield a vanishing result since the corresponding expression equals the term of order $\gamma^2\lambda$ of an expansion of

$$\left\langle T_K\left[\exp\left(-\frac{i}{\hbar}\sum_{\eta'=\pm}\eta'\int_{-\infty}^{\infty}dt'\mathcal{H}_1^{(\eta')}(t')\right)\right]\right\rangle_0 \equiv 1. \tag{A18}$$

Simple transformations of the integration variables of Eq. (A14) and use of the relations

$$\int_{-\infty}^{\infty}dt\langle\partial_x\Theta(x,t)\Phi_r(x_0,0)\rangle_0^{\mathrm{Kel}} = 0, \tag{A19}$$

$$\int_{-\infty}^{\infty}dt\langle\partial_x\Theta(x,t)\Phi_r(x_0,0)\rangle_0^{\mathrm{ret}} = \frac{\mathrm{i}}{4v_{\mathrm{W}}}[1+r\,\mathrm{sgn}(x-x_0)] \tag{A20}$$

obtained from the correlation functions provided in Appendix C, yield

$$I_{\gamma^2\lambda}(x,t) = -\frac{ev_W^3 v_T}{16\pi^3 a_T a_W^2}\gamma_+\gamma_-\sum_{i=1,2}\lambda_i\int\int dt_1 dt_2 \Im\Big\{e^{ie[(V_S+V_D-2V_T)(t_1-t_2)+(V_S-V_D)(t_1-t_3+t_2-t_3)]/2\hbar}e^{-2i[k_W+g^2e(V_S+V_D-2V_G)/\hbar v_W](x_0-x_i)}$$
$$\times\sum_{\eta_1,\eta_2,\eta_3=\pm}\eta_1\eta_2\eta_3 F_W^{\eta_1\eta_2\eta_3}(t_1,t_2)F_T^{\eta_1\eta_2}(t_1-t_2)b_{W,\gamma^2\lambda,i}^{\eta_1\eta_2\eta_3}(t_1,t_2)b_{T,\gamma^2\lambda,i}^{\eta_1\eta_2}(t_1-t_2)[\eta_1+\eta_2-2\eta_3+\mathrm{sgn}(x-x_0)(\eta_1-\eta_2)]\Big\}. \tag{A21}$$

Taking into account Eqs. (B8), (B16), (B24), and (B26), we now observe that upon reversal of Keldysh contour indices $\eta_i\to-\eta_i$ $(i=1,2,3)$,

$$F_W^{\eta_1\eta_2\eta_3}(t_1,t_2)\to F_W^{\eta_1\eta_2\eta_3}(t_1,t_2), \tag{A22}$$

$$F_T^{\eta_1\eta_2}(t_1-t_2)\to -F_T^{\eta_1\eta_2}(t_1-t_2), \tag{A23}$$

$$b_{W,\gamma^2\lambda,i}^{\eta_1\eta_2\eta_3}(t_1,t_2)\to[b_{W,\gamma^2\lambda,i}^{\eta_1\eta_2\eta_3}(t_1,t_2)]^*, \tag{A24}$$

$$b_{T,\gamma^2}^{\eta_1\eta_2}(t_1-t_2)\to[b_{T,\gamma^2}^{\eta_1\eta_2}(t_1-t_2)]^*, \tag{A25}$$

implying that in Eq. (A21) the contribution for $\eta_3=-$ is conjugate to the one stemming from $\eta_3=+$. Thus

$$I_{\gamma^2\lambda}(x,t) = -\frac{ev_W^3 v_T}{8\pi^3 a_T a_W^2}\gamma_+\gamma_-\sum_{i=1,2}\lambda_i\int\int dt_1 dt_2 \Im\Big\{e^{ie[(V_S+V_D-2V_T)(t_1-t_2)+(V_S-V_D)(t_1+t_2)]/2\hbar}e^{-2i[k_W+g^2e(V_S+V_D-2V_G)/\hbar v_W](x_0-x_i)}$$
$$\times\sum_{\eta_1,\eta_2=\pm}F_W^{\eta_1\eta_2+}(t_1,t_2)F_T^{\eta_1\eta_2}(t_1-t_2)b_{W,\gamma^2\lambda,i}^{\eta_1\eta_2+}(t_1,t_2)b_{T,\gamma^2}^{\eta_1\eta_2}(t_1-t_2)[\eta_2+\eta_1-2\eta_1\eta_2+\mathrm{sgn}(x-x_0)(\eta_2-\eta_1)]\Big\}. \tag{A26}$$

The term $\mathrm{sgn}(x-x_0)$ appearing in the last line is positive (negative) for a measurement point x located in the drain (source) lead. Recalling that the current can be written as in Eqs. (16) and (17), it is easily seen that those terms that are multiplied by $\mathrm{sgn}(x-x_0)$ yield $I_T/2$, whereas the other ones yield I_M. Inserting Eqs. (B8), (B16), (B24), and (B26) into Eq. (A26) and changing to dimensionless integration variables $\tau_i=tv_W/gL$, result (69) is obtained.

Similar procedures can be applied to evaluate the terms of orders λ^2, λ^3, and γ^2. We find

$$I_{\lambda^2}(x,t) = -\frac{ev_W^3}{2}\sum_{i,j=1,2}\lambda_i\lambda_j\int\int dt_1 dt_2$$
$$\times\sum_{\eta_1,\eta_2=\pm}\eta_1\eta_2\Re\{W_{\lambda^2,ij}^{\eta_1\eta_2}(t_1,t_2)e^{-2ik_W(x_i-x_j)}\}, \tag{A27}$$

$$I_{\lambda^3}(x,t) = -\frac{ev_W^4}{2}\sum_{i,j,k=1,2}\lambda_i\lambda_j\lambda_k\int\int\int dt_1 dt_2 dt_3$$
$$\times\sum_{\eta_1,\eta_2=\pm}\eta_1\eta_2\Im\{W_{\lambda^3,ijk}^{\eta_1\eta_2}(t_1,t_2,t_3)e^{-2ik_W(x_i-x_j)}\}, \tag{A28}$$

and

$$I_{\gamma^2}(x,t) = -\frac{ev_W^2 v_T}{2}\sum_{r=\pm}\gamma_r^2\int\int dt_1 dt_2$$
$$\times\sum_{\eta_1,\eta_2=\pm}\eta_1\eta_2\Re\{W_{\gamma^2,r}^{\eta_1\eta_2}(t_1,t_2)T_{\gamma^2}^{\eta_1\eta_2}(t_1,t_2)\}, \tag{A29}$$

where

$$W_{\lambda^2,ij}^{\eta_1\eta_2}(t_1,t_2) = \sum_{\eta=\pm}\langle T_K[j^{(\eta)}(x,t)\mathcal{U}_W\Psi_+^{\dagger(\eta_1)}(x_i,t_1)\Psi_-^{(\eta_1)}(x_i,t_1)$$
$$\times\Psi_-^{\dagger(\eta_2)}(x_j,t_2)\Psi_+^{(\eta_2)}(x_j,t_2)]\rangle_0, \tag{A30}$$

$$W_{\lambda^3,ijk}^{\eta_1\eta_2}(t_1,t_2,t_3) = \sum_{\eta,\eta_3,r=\pm}\eta_3\langle T_K[j^{(\eta)}(x,t)\mathcal{U}_W\Psi_+^{\dagger(\eta_1)}(x_i,t_1)$$
$$\times\Psi_-^{(\eta_1)}(x_i,t_1)\Psi_-^{\dagger(\eta_2)}(x_j,t_2)\Psi_+^{(\eta_2)}(x_j,t_2)$$
$$\times\rho_r^{(\eta_3)}(x_k,t_3)]\rangle_0, \tag{A31}$$

and

$$W_{\gamma^2,r}^{\eta_1\eta_2}(t_1,t_2) = \sum_{\eta=\pm}\langle T_K[j^{(\eta)}(x,t)\mathcal{U}_W\Psi_r^{\dagger(\eta_1)}(x_0,t_1)$$
$$\times\Psi_r^{(\eta_2)}(x_0,t_2)]\rangle_0. \tag{A32}$$

APPENDIX B: EVALUATION OF W AND T FACTORS BY BOSONIZATION

Hamiltonian (A3) of the interaction picture decomposes into commuting wire and tip parts, i.e., $\mathcal{H}_0=\mathcal{H}_{0,\mathrm{W}}+\mathcal{H}_{0,\mathrm{T}}$. For a noninteracting wire $\mathcal{H}_{0,\mathrm{W}}=\mathcal{H}_{\mathrm{kin,W}}$ and the wire correlation functions W introduced in Eqs. (A12) and (A30)–(A32) can be factorized into products of single-particle electron correlators using Wick's theorem. In this case the W's can be evaluated straightforwardly, and the results for contributions (A11) and (A27)–(A29) to the current coincide with the corresponding terms of an expansion of the current obtained from the scattering matrix formalism. In the interacting case, however, $\mathcal{H}_{0,\mathrm{W}}=\mathcal{H}_{\mathrm{kin,W}}+\mathcal{H}_U$, and Wick's theorem cannot be applied. In this appendix we evaluate the wire correlators W using the bosonization technique.[41] The wire field operators can be represented as

$$\Psi_r(x)=\frac{\kappa_r}{\sqrt{2\pi a_{\mathrm{W}}}}e^{ir\sqrt{4\pi}\Phi_r(x)}, \tag{B1}$$

where the fields $\Phi_\pm$ describe particle-hole excitations and κ_r are the Klein factors represented as Majorana fermions.[41] Finally, a_{W} is a cut-off length of order of the lattice spacing.

Introducing Eq. (B1) into Eqs. (3) and (13), one obtains

$$\mathcal{H}_{0,\mathrm{W}}=\frac{\hbar v_{\mathrm{W}}}{2}\int_{-\infty}^{\infty}dx\left\{:\Pi^2(x)+\frac{1}{g^2(x)}[\partial_x\Phi(x)]^2:\right\}, \tag{B2}$$

where $\Phi=\Phi_+ +\Phi_-$ and $\Pi=-\partial_x(\Phi_+-\Phi_-)$ are the conjugate bosonic fields, i.e., $[\Phi(x,t),\Pi(y,t)]=\mathrm{i}\delta(x-y)$. Finally,

$$g(x)=\begin{cases}1 & \text{for } |x|>L/2\\ \left(1+\dfrac{U}{\pi\hbar v_{\mathrm{W}}}\right)^{-1/2} & \text{for } |x|<L/2\end{cases} \tag{B3}$$

is the inhomogeneous interaction parameter. Notice that $0\le g\le 1$, where $g=1$ describes the noninteracting case present in the leads. The limit $g\to 0$ corresponds to strongly repulsive interaction. The wire current operator Eq. (14) is expressed in terms of the dual field $\Theta=\Phi_+-\Phi_-$ as

$$I(x,t)=ev_{\mathrm{W}}\langle\partial_x\Theta(x,t)\rangle. \tag{B4}$$

Further, with the help of the relation

$$\rho_r(x,t)=\frac{\partial_x\Phi_r(x,t)}{\sqrt{\pi}}, \tag{B5}$$

term (6) of the Hamiltonian can be written as

$$\mathcal{H}_{\mu_{\mathrm{W}}}=\frac{1}{\sqrt{\pi}}\int_{-\infty}^{+\infty}dx\mu_{\mathrm{W}}(x)\partial_x\Phi(x). \tag{B6}$$

We start by discussing the derivation of $\mathrm{W}^{\eta_1\eta_2\eta_3}_{\gamma^2\lambda,i}(t_1,t_2,t_3)$. Inserting Eqs. (B1), (B4), and (B5) into Eq. (A11), one obtains

$$\mathrm{W}^{\eta_1\eta_2\eta_3}_{\gamma^2\lambda,i}(t_1,t_2,t_3)=\frac{1}{(2\pi a_{\mathrm{W}})^2}F^{\eta_1\eta_2\eta_3}_{\mathrm{W}}(t_1-t_3,t_2-t_3)\times B^{\eta_1\eta_2\eta_3}_{\mathrm{W},\gamma^2\lambda,i}(t_1,t_2,t_3). \tag{B7}$$

Here

$$\begin{aligned}F^{\eta_1\eta_2\eta_3}_{\mathrm{W}}(t_1-t_3,t_2-t_3)&=\langle T_K[\kappa_+^{(\eta_1)}(t_1)\kappa_-^{(\eta_2)}(t_2)\kappa_-^{(\eta_3)}(t_3)\kappa_+^{(\eta_3)}(t_3)]\rangle_0\\&=\theta(t_3-t_1)\theta(t_3-t_2)\eta_1\eta_2+\theta(t_1-t_3)\theta(t_2-t_3)\\&\quad-\theta(t_2-t_3)\theta(t_3-t_1)\eta_1\eta_3-\theta(t_1-t_3)\theta(t_3-t_2)\eta_2\eta_3\end{aligned} \tag{B8}$$

accounts for the correlation function of fermionic Klein factors, whereas

$$B^{\eta_1\eta_2\eta_3}_{\mathrm{W},\gamma^2\lambda,i}(t_1,t_2,t_3)=\sum_{\eta=\pm}\frac{\delta}{\delta J^{(\eta)}_\Theta(x,t)}\left\langle T_K\left\{\exp\left(-\frac{i}{\hbar}\sum_{\eta'=\pm}\eta'\int d\mathbf{x}'\mu_{\mathrm{W}}(x')\frac{\partial_{x'}\Phi^{(\eta')}(\mathbf{x}')}{\sqrt{\pi}}+\sum_{\eta''=\pm}\int d\mathbf{x}''J^{(\eta'')}_\Theta(\mathbf{x}'')\frac{\partial_x\Theta^{(\eta'')}(\mathbf{x}'')}{\sqrt{\pi}}\right.\right.\right.$$
$$\left.\left.\left.-i\sqrt{4\pi}[\Phi^{(\eta_1)}_+(x_0,t_1)+\Phi^{(\eta_2)}_-(x_0,t_2)-\Phi^{(\eta_3)}(x_i,t_3)]\right)\right\}\right\rangle_0\Bigg|_{J_\Theta\equiv 0} \tag{B9}$$

correlates bosonic vertex operators. Also, we have introduced the notation $\mathbf{x}=(x,t)$. Expression (B9) can straightforwardly be evaluated taking into account that for a functional

$$\zeta[J]=\left\langle T_K\left\{\exp\left(A+\sum_{\eta=\pm}\int d\mathbf{x}J^{(\eta)}(\mathbf{x})B^{(\eta)}(\mathbf{x})\right)\right\}\right\rangle_0, \tag{B10}$$

where A and B are linear combinations of bosonic operators, one has[41]

$$\left.\frac{\delta\zeta[J]}{\delta J^{(\eta)}(\mathbf{x})}\right|_{J=0} = \langle T_K[AB^{(\eta)}(\mathbf{x})]\rangle_0 \exp\{\langle T_K(A^2)\rangle_0\}. \tag{B11}$$

Furthermore, it can be shown that $\mathcal{H}_{\mu_W}$, i.e., the first term appearing in the exponent of Eq. (B9), simply yields a shift in the operators $\Phi_\pm$ according to

$$\Phi_r^{(\eta)}(x,t) \to \Phi_r^{(\eta)}(x,t) + \Phi_{0,r}(x,t) \quad r = \pm, \tag{B12}$$

where the zero modes,

$$\Phi_{0,r}(x,t) = -\frac{1}{4\sqrt{\pi}}\frac{e[V_S - V_D + r(V_S + V_D)]}{\hbar}t + \frac{e}{4\sqrt{\pi}\hbar v_W}\begin{cases} -(V_S - V_D)\left[(1-r)x + \frac{L}{2}\right] - g^2(V_S + V_D - 2V_G)\frac{L}{2} & \text{for } x \le -L/2 \\ [g^2(V_S + V_D - 2V_G) + r(V_S - V_D)]x & \text{for } |x| \le L/2 \\ (V_S - V_D)\left[(1+r)x - \frac{L}{2}\right] + g^2(V_S + V_D - 2V_G)\frac{L}{2} & \text{for } x \ge L/2, \end{cases} \tag{B13}$$

fulfill the equation,

$$\Phi_{0,r}(\mathbf{x}) - \Phi_{0,r}(\mathbf{y}) = \frac{-i}{\sqrt{\pi}\hbar}\int d\mathbf{x}'\,\mu_W(\mathbf{x}')[\langle\Phi_r(\mathbf{x})\partial_x\Phi(\mathbf{x}')\rangle^{\text{ret}} - \langle\Phi_r(\mathbf{y})\partial_x\Phi(\mathbf{x}')\rangle^{\text{ret}}]. \tag{B14}$$

After lengthy but straightforward algebra one obtains

$$\begin{aligned} B^{\eta_1\eta_2\eta_3}_{W,\gamma^2\lambda,i}(t_1,t_2,t_3) = &-2ie^{(ie/\hbar)[V_S(t_1-t_3) - V_D(t_2-t_3) - g^2(V_S+V_D-2V_G)(x_0-x_i)/v_W]} b^{\eta_1\eta_2\eta_3}_{W,\gamma^2\lambda,i}(t_1-t_3,t_2-t_3) \\ &\times\Big\{\langle\partial_x\Theta(x,t)\Phi_+(x_0,t_1)\rangle_0^{\text{Kel}} + \eta_1\langle\partial_x\Theta(x,t)\Phi_+(x_0,t_1)\rangle_0^{\text{ret}} + \langle\partial_x\Theta(x,t)\Phi_-(x_0,t_2)\rangle_0^{\text{Kel}} + \eta_2\langle\partial_x\Theta(x,t)\Phi_-(x_0,t_2)\rangle_0^{\text{ret}} \\ &- \langle\partial_x\Theta(x,t)\Phi(x_i,t_3)\rangle_0^{\text{Kel}} - \eta_3\langle\partial_x\Theta(x,t)\Phi(x_i,t_2)\rangle_0^{\text{ret}} + \frac{1}{\pi\hbar}\int d\mathbf{x}'\,\mu_W(x')\langle T_K[\partial_x\Theta(x,t)\partial_{x'}\Phi(\mathbf{x}')]\rangle_0^{\text{ret}}\Big\}, \end{aligned} \tag{B15}$$

where

$$\begin{aligned} b^{\eta_1\eta_2\eta_3}_{W,\gamma^2\lambda,i}(t_1,t_2) &= \exp\{-2\pi\langle T_K\{[\Phi_+^{(\eta_1)}(x_0,t_1) + \Phi_-^{(\eta_2)}(x_0,t_2) \\ &\quad - \Phi^{(\eta_3)}(x_i,0)]^2\}\rangle_0\} \\ &= \exp\{4\pi[\mathcal{R}_W(\xi_0;\xi_i;\tau_1;\tau_2) \\ &\quad + i\mathcal{I}_W^{\eta_1\eta_2\eta_3}(\xi_0;\xi_i;\tau_1;\tau_2)]\}. \end{aligned} \tag{B16}$$

The correlation functions $\mathcal{R}_W(\xi_0;\xi_i;\tau_1;\tau_2)$ and $\mathcal{I}_W^{\eta_1\eta_2\eta_3}(\xi_0;\xi_i;\tau_1;\tau_2)$ are defined in Appendix C [see Eqs. (C1)–(C6)] and also given explicitly there in the zero temperature limit. The arguments $\tau_i = t_i v_W/gL = t_i\omega_L^*$ and $\xi_j = x_j/L$ $(j=0,1,2)$ are dimensionless time and space variables. In deriving Eqs. (B15) and (B16) we have used the equalities

$$\begin{aligned} &\langle T_K[A^{(\eta_A)}(t_A)B^{(\eta_B)}(t_B)]\rangle \\ &= \frac{1}{2}[\langle A(t_A)B(t_B)\rangle^{\text{Kel}} + \eta_A\langle A(t_A)B(t_B)\rangle^{\text{adv}} \\ &\quad + \eta_B\langle A(t_A)B(t_B)\rangle^{\text{ret}}] \end{aligned} \tag{B17}$$

and

$$\begin{aligned} \langle A(t_A)B(t_B)\rangle^{\text{Kel}} &= \frac{1}{2}\sum_{\eta_A,\eta_B=\pm}\langle A^{(\eta_A)}(t_A)B^{(\eta_B)}(t_B)\rangle \\ &= 2\Re\langle A(t_A)B(t_B)\rangle, \end{aligned} \tag{B18}$$

$$\begin{aligned} \langle A(t_A)B(t_B)\rangle^{\text{ret}} &= \frac{1}{2}\sum_{\eta_A,\eta_B=\pm}\eta_B\langle A^{(\eta_A)}(t_A)B^{(\eta_B)}(t_B)\rangle \\ &= 2i\theta(t_A - t_B)\Im\langle A(t_A)B(t_B)\rangle, \end{aligned} \tag{B19}$$

$$\begin{aligned} \langle A(t_A)B(t_B)\rangle^{\text{adv}} &= \frac{1}{2}\sum_{\eta_A,\eta_B=\pm}\eta_A\langle A^{(\eta_A)}(t_A)B^{(\eta_B)}(t_B)\rangle \\ &= -2i\theta(t_B - t_A)\Im\langle A(t_A)B(t_B)\rangle, \end{aligned} \tag{B20}$$

valid for any pair A and B of real Bose operators.

As far as the tip correlators T are concerned, see Eqs. (A13), (A29), and (A27), Wick's theorem might be applied since the tip is supposed to be noninteracting, and the use of bosonization is unnecessary. However, to have a uniform formalism and notation throughout the paper, we prefer to utilize a bosonized approach for the tip as well. The tip electron field and density are written as

$$c(y) = \frac{\kappa_T}{\sqrt{2\pi a_T}} e^{i\sqrt{4\pi}\varphi(y)} \tag{B21}$$

and

$$:c^\dagger(y)c(y): = \frac{\partial_y \varphi(y)}{\sqrt{\pi}}, \tag{B22}$$

where $\varphi(y)$ is a chiral (right-moving) boson field and κ_T and a_T are the Klein factor and cut-off length of the tip, respectively. By way of example, we evaluate here the T factor [Eq. (A13)] appearing in the calculation of $I_{\gamma^2\lambda}$. Inserting Eqs. (B21) and (B22) into Eqs. (A6) and (A13), one obtains

$$T_{\gamma^2}^{\eta_1\eta_2}(t_1 - t_2) = \frac{1}{2\pi a_T} F_T^{\eta_1\eta_2}(t_1 - t_2) B_{T,\gamma^2}^{\eta_1\eta_2}(t_1 - t_2), \tag{B23}$$

where, similar to the wire case,

$$\begin{aligned} F_T^{\eta_1\eta_2}(t_1 - t_2) &= \langle T_K[\kappa_T^{(\eta_1)}(t_1), \kappa^{(\eta_2)}(t_2)]\rangle_0 \\ &= -\eta_1\theta(t_2 - t_1) + \eta_2\theta(t_1 - t_2) \end{aligned} \tag{B24}$$

accounts for the correlation function of fermionic Klein factors, whereas the correlator of bosonic vertex operators reads

$$B_{T,\gamma^2}^{\eta_1\eta_2}(t_1 - t_2) = \left\langle T_K\left[\exp\left(-\frac{i}{\hbar}\sum_{\eta'=\pm}\eta'\int d\mathbf{y}'\mu_T(y')\frac{\partial_{y'}\varphi(\mathbf{y}')}{\sqrt{\pi}} + i\sqrt{4\pi}[\varphi^{(\eta_1)}(0,t_1) - \varphi^{(\eta_2)}(0,t_2)]\right)\right]\right\rangle_0. \tag{B25}$$

It is easily verified that the first term in the exponential function, which originates from term (12) in the Hamiltonian, merely yields a time-dependent phase factor so that

$$B_{T,\gamma^2}^{\eta_1\eta_2}(t_1 - t_2) = e^{-(ie/\hbar)V_T(t_1 - t_2)} b_{T,\gamma^2}^{\eta_1\eta_2}(t_1 - t_2), \tag{B26}$$

where

$$\begin{aligned} b_{T,\gamma^2}^{\eta_1\eta_2}(t_1 - t_2) &= \exp\{-2\pi\langle T_K[(\varphi^{(\eta_1)}(0,t_1) - \varphi^{(\eta_2)}(0,t_2))^2]\rangle_0\} \\ &= \exp\{4\pi[\mathcal{R}_T(\tau_1 - \tau_2) + i\mathcal{I}_T^{\eta_1\eta_2}(\tau_1 - \tau_2)]\}. \end{aligned} \tag{B27}$$

The functions $\mathcal{R}_T(\tau)$ and $\mathcal{I}_T^{\eta_1\eta_2}(\tau)$ are given in Appendix C, see Eqs. (C12).

APPENDIX C: CORRELATION FUNCTIONS

This appendix collects properties of correlation functions appearing in Eqs. (60) and (69), as well as in Eqs. (B16) and (B27). The transport properties of the wire are expressed in terms of the functions

$$\begin{aligned} \mathcal{R}_W(\xi_0;\xi_i;\tau_1;\tau_2) &= \mathcal{R}_{reg}^{\Phi_+\Phi_+}(\xi_0;\xi_i;\tau_1) + \mathcal{R}_{reg}^{\Phi_-\Phi_-}(\xi_0;\xi_i;\tau_2) \\ &+ \mathcal{R}^{\Phi_+\Phi_-}(\xi_0;\xi_i;\tau_1) + \mathcal{R}^{\Phi_-\Phi_+}(\xi_0;\xi_i;\tau_2) \\ &- \mathcal{R}^{\Phi_+\Phi_-}(\xi_0;\xi_0;\tau_1 - \tau_2) - \mathcal{R}^{\Phi_-\Phi_+}(\xi_i;\xi_i;0), \end{aligned} \tag{C1}$$

$$\begin{aligned} \mathcal{I}_W^{\eta_1\eta_2\eta_3}(\xi_0;\xi_i;\tau_1;\tau_2) &= \sum_{r=\pm}\{[\eta_3\theta(\tau_1) - \eta_1\theta(-\tau_1)]\mathcal{I}^{\Phi_+\Phi_r}(\xi_0;\xi_i;\tau_1) \\ &+ [\eta_3\theta(\tau_2) - \eta_2\theta(-\tau_2)]\mathcal{I}^{\Phi_-\Phi_r}(\xi_0;\xi_i;\tau_2)\} \\ &- [\eta_2\theta(\tau_1 - \tau_2) - \eta_1\theta(\tau_2 - \tau_1)]\mathcal{I}^{\Phi_+\Phi_-}(\xi_0;\xi_0;\tau_1 - \tau_2), \end{aligned} \tag{C2}$$

where the functions $\mathcal{R}_{reg}^{\Phi_r\Phi_r}(\xi;\xi';\tau)$ and $\mathcal{I}^{\Phi_r\Phi_r}(\xi;\xi';\tau)$ are the real and imaginary parts, respectively, of the autocorrelation functions of the bosonic fields Φ_r. Specifically

$$\mathcal{R}_{reg}^{\Phi_r\Phi_r}(\xi;\xi';\tau) = \Re\left\{\left\langle \Phi_r(x,t)\Phi_r(x',0) - \frac{1}{2}[\Phi_r^2(x,t) + \Phi_r^2(x',0)]\right\rangle_0\right\}, \tag{C3}$$

$$\mathcal{I}^{\Phi_r\Phi_r}(\xi;\xi';\tau) = \Im\{\langle\Phi_r(x,t)\Phi_r(x',0)\rangle_0\}. \tag{C4}$$

Likewise, the real and imaginary parts of the crosscorrelation functions of fields with different chirality r read

$$\mathcal{R}^{\Phi_r\Phi_{-r}}(\xi;\xi';\tau) = \Re\{\langle\Phi_r(x,t)\Phi_{-r}(y,0)\rangle_0\}, \tag{C5}$$

$$\mathcal{I}^{\Phi_r\Phi_{-r}}(\xi;\xi';\tau) = \Im\{\langle\Phi_r(x,t)\Phi_{-r}(y,0)\rangle_0\}. \tag{C6}$$

Notice that the real part of the correlation functions of fields with the same chirality needs to be defined with an infrared regularization as in Eq. (C3). The above equations are given in terms of the dimensionless time and space variables $\tau = tv_W/gL$ and $\xi = x/L$ introduced previously. From the inhomogeneous Luttinger liquid model one obtains at zero temperature

$$\begin{aligned} \mathcal{R}_{reg}^{\Phi_r\Phi_r}(\xi,\xi',\tau) = -\frac{1}{32\pi}\Bigg\{ &(g + g^{-1} - 2r)\sum_{m\in Z_{even}}\rho^{|m|}\ln\frac{\alpha_W^2 + (\tau + \xi_r + m)^2}{\alpha_W^2 + m^2} + (g + g^{-1} + 2r)\sum_{m\in Z_{even}}\rho^{|m|}\ln\frac{\alpha_W^2 + (\tau - \xi_r - m)^2}{\alpha_W^2 + m^2} \\ &+ (g - g^{-1})\sum_{m\in Z_{odd}}\rho^{|m|}\left(\ln\frac{\alpha_W^2 + (\tau + \xi_R + m)^2}{\alpha_W^2 + (\xi_R + m)^2} + \ln\frac{\alpha_W^2 + (\tau - \xi_R - m)^2}{\alpha_W^2 + (\xi_R + m)^2} + \ln\frac{[\alpha_W^2 + (\xi_R + m)^2]^2}{[\alpha_W^2 + (2\xi + m)^2][\alpha_W^2 + (2\xi' + m)^2]}\right)\Bigg\}, \end{aligned} \tag{C7}$$

$$\mathcal{I}^{\Phi_r\Phi_r}(\xi,\xi',\tau) = -\frac{1}{16\pi}\Bigg\{(g+g^{-1}-2r)\sum_{m\in Z_{\text{even}}}\rho^{|m|}\arctan\left(\frac{\tau+\xi_r+m}{\alpha_W}\right)+(g+g^{-1}+2r)\sum_{m\in Z_{\text{even}}}\rho^{|m|}\arctan\left(\frac{\tau-\xi_r-m}{\alpha_W}\right)$$
$$+(g-g^{-1})\sum_{m\in Z_{\text{odd}}}\rho^{|m|}\left[\arctan\left(\frac{\tau+\xi_R+m}{\alpha_W}\right)+\arctan\left(\frac{\tau-\xi_R-m}{\alpha_W}\right)\right]\Bigg\}, \tag{C8}$$

$$\mathcal{R}^{\Phi_r\Phi_{-r}}(\xi;\xi';\tau) = -\frac{1}{32\pi}\Bigg\{(g-g^{-1})\sum_{m\in Z_{\text{even}}}\rho^{|m|}\left[\ln\left(\frac{\alpha_W^2+(\tau+\xi_r+m)^2}{\alpha_W^2+m^2}\right)+\ln\left(\frac{\alpha_W^2+(\tau-\xi_r-m)^2}{\alpha_W^2+m^2}\right)\right]$$
$$+(g+g^{-1}-2r)\sum_{m\in Z_{\text{odd}}}\rho^{|m|}\ln\left(\frac{\alpha_W^2+(\tau+\xi_R+m)^2}{\alpha_W^2+(\xi_R+m)^2}\right)+(g+g^{-1}+2r)\sum_{m\in Z_{\text{odd}}}\rho^{|m|}\ln\left(\frac{\alpha_W^2+(\tau-\xi_R-m)^2}{\alpha_W^2+(\xi_R+m)^2}\right)$$
$$+(g+g^{-1})\sum_{m\in Z_{\text{odd}}}\rho^{|m|}\ln\frac{[\alpha_W^2+(\xi_R+m)^2]^2}{[\alpha_W^2+(2\xi+m)^2][\alpha_W^2+(2\xi'+m)^2]}-\frac{1}{2}(g-g^{-1})\sum_{m\in Z_{\text{even}}}\rho^{|m|}$$
$$\times\left[\ln\left(\frac{[\alpha_W^2+(2\xi+1+m)^2][\alpha_W^2+(2\xi'+1+m)^2]}{(\alpha_W^2+m^2)^2}\right)+\ln\left(\frac{[\alpha_W^2+(2\xi-1+m)^2][\alpha_W^2+(2\xi'-1+m)^2]}{(\alpha_W^2+m^2)^2}\right)\right]\Bigg\} \tag{C9}$$

and

$$\mathcal{I}^{\Phi_r\Phi_{-r}}(\xi;\xi';\tau) = -\frac{1}{16\pi}\Bigg\{(g-g^{-1})\sum_{m\in Z_{\text{even}}}\rho^{|m|}\left[\arctan\left(\frac{\tau+\xi_r+m}{\alpha_W}\right)+\arctan\left(\frac{\tau-\xi_r-m}{\alpha_W}\right)\right]$$
$$+(g+g^{-1}-2r)\sum_{m\in Z_{\text{odd}}}\rho^{|m|}\arctan\left(\frac{\tau+\xi_R+m}{\alpha_W}\right)+(g+g^{-1}+2r)\sum_{m\in Z_{\text{odd}}}\rho^{|m|}\arctan\left(\frac{\tau-\xi_R-m}{\alpha_W}\right)\Bigg\}. \tag{C10}$$

Here we have introduced $\xi_r=\xi-\xi'$, $\xi_R=\xi+\xi'$, and the dimensionless cut-off length $\alpha_W=a_W/gL$, as well as the Andreev-type reflection coefficient $\rho=(1-g)/(1+g)$.

The correlation functions for the noninteracting tip can directly be obtained from the above results. The tip is described by a single chiral mode, and we need the correlation function only for coordinates at the injection point $y=0$. From Eqs. (C7) and (C8) we find for $\xi=\xi'=0$ by taking the limit $g\to 1$ and replacing α_W by α_T

$$\mathcal{R}_T(\tau)=\mathcal{R}^{\varphi\varphi}_{\text{reg}}(0;0;\tau)=\mathcal{R}^{\Phi_+\Phi_+}_{\text{reg}}(0;0;\tau)\big|^{g\to 1}_{\alpha_W\to\alpha_T}=-\frac{1}{8\pi}\ln\frac{\alpha_T^2+\tau^2}{\alpha_T^2}, \tag{C11}$$

$$\mathcal{I}^{\eta_1\eta_2}_T(\tau)=F^{\eta_1\eta_2}_T(\tau)\mathcal{I}^{\varphi\varphi}(0;0;\tau)=F^{\eta_1\eta_2}_T(\tau)\mathcal{I}^{\Phi_+\Phi_+}(0;0;\tau)\big|^{g\to 1}_{\alpha_W\to\alpha_T}=-\frac{\eta_2\theta(\tau)-\eta_1\theta(-\tau)}{4\pi}\arctan\left(\frac{\tau}{\alpha_T}\right). \tag{C12}$$

[1] Z. Zhang and C. M. Lieber, Appl. Phys. Lett. **62**, 2792 (1993); J. W. G. Wilder, L. C. Venema, A. G. Rinzler, R. E. Smalley, and C. Dekker, Nature (London) **391**, 59 (1998); T. W. Odom, J.-L. Huang, P. Kim, and C. M. Lieber, *ibid.* **391**, 62 (1998); M. A. Topinka, B. J. LeRoy, S. E. J. Shaw, E. J. Heller, R. M. Westervelt, K. D. Maranowski, and A. C. Gossard, Science **289**, 2323 (2000); B. J. LeRoy, I. Heller, V. K. Pahilwani, C. Dekker, and S. G. Lemay, Nano Lett. **7**, 2937 (2007).

[2] A. Yazdani, B. A. Jones, C. P. Lutz, M. F. Crommie, and D. M. Eigler, Science **275**, 1767 (1997); S. H. Pan, E. W. Hudson, and J. C. Davis, Appl. Phys. Lett. **73**, 2992 (1998); T. Proslier, A. Kohen, Y. Noat, T. Cren, D. Roditchev, and W. Sacks, Europhys. Lett. **73**, 962 (2006); A. Kohen, Th. Proslier, T. Cren, Y. Noat, W. Sacks, H. Berger, and D. Roditchev, Phys. Rev. Lett. **97**, 027001 (2006).

[3] B. J. van Wees, K.-M. H. Lenssen, and C. J. P. M. Harmans, Phys. Rev. B **44**, 470 (1991); A. F. Volkov, Phys. Rev. Lett. **74**, 4730 (1995); F. K. Wilhelm, G. Schön, and A. D. Zaikin, *ibid.* **81**, 1682 (1998); J. J. A. Baselmans, A. F. Morpurgo, B. J. van Wees, and T. M. Klapwijk, Nature (London) **397**, 43 (1999); P. Samuelsson, J. Lantz, V. S. Shumeiko, and G. Wendin, Phys. Rev. B **62**, 1319 (2000); F. Giazotto, T. T. Heikkilä, A. Luukanen, A. M. Savin, and J. P. Pekola, Rev. Mod. Phys. **78**, 217 (2006).

[4] M. Woodside and P. McEuen, Science **296**, 1098 (2002).

[5] A. Naik, O. Buu, M. D. LaHaye, A. D. Armour, A. A. Clerk, M. P. Blencowe, and K. C. Schwab, Nature (London) **443**, 193 (2006); R. Ruskov, K. Schwab, and A. N. Korotkov, Phys. Rev. B **71**, 235407 (2005).

[6] M. Büttiker, Y. Imry, and M. Ya. Azbel, Phys. Rev. A **30**, 1982

(1984); F. Marquardt and C. Bruder, Phys. Rev. B **70**, 125305 (2004); F. Marquardt, *ibid.* **74**, 125319 (2006).

[7] C. Texier and M. Büttiker, Phys. Rev. B **62**, 7454 (2000); S. Pilgram, P. Samuelsson, H. Förster, and M. Büttiker, Phys. Rev. Lett. **97**, 066801 (2006); H. Förster, P. Samuelsson, and M. Büttiker, N. J. Phys. **9**, 117 (2007).

[8] A. Yacoby, H. L. Stormer, K. W. Baldwin, L. N. Pfeiffer, and K. W. West, Solid State Commun. **101**, 77 (1997); R. de Picciotto, H. L. Stormer, L. N. Pfeiffer, K. W. Baldwin, and K. W. West, Nature (London) **411**, 51 (2001).

[9] C. T. White and T. N. Torodov, Nature (London) **393**, 240 (1998).

[10] W. Liang, M. Bockrath, D. Bozovic, J. H. Hafner, M. Tinkham, and H. Park, Nature (London) **411**, 665 (2001).

[11] A. Yacoby, H. L. Stormer, N. S. Wingreen, L. N. Pfeiffer, K. W. Baldwin, and K. W. West, Phys. Rev. Lett. **77**, 4612 (1996); O. M. Auslaender, A. Yacoby, R. de Picciotto, K. W. Baldwin, L. N. Pfeiffer, and K. W. West, *ibid.* **84**, 1764 (2000).

[12] O. M. Auslaender, H. Steinberg, A. Yacoby, Y. Tserkovnyak, B. I. Halperin, K. W. Baldwin, L. N. Pfeiffer, and K. W. West, Science **308**, 88 (2005); H. Steinberg, O. M. Auslaender, A. Yacoby, J. Qian, G. A. Fiete, Y. Tserkovnyak, B. I. Halperin, K. W. Baldwin, L. N. Pfeiffer, and K. W. West, Phys. Rev. B **73**, 113307 (2006).

[13] M. Bockrath, D. H. Cobden, J. Lu, A. G. Rinzler, R. E. Smalley, L. Balents, and P. L. McEuen, Nature (London) **397**, 598 (1999); Z. Yao, H. W. Ch. Postma, L. Balents, and C. Dekker, *ibid.* **402**, 273 (1999).

[14] N. Y. Kim, P. Recher, W. D. Oliver, Y. Yamamoto, J. Kong, and H. Dai, Phys. Rev. Lett. **99**, 036802 (2007).

[15] S. Eggert, Phys. Rev. Lett. **84**, 4413 (2000).

[16] I. Ussishkin and L. I. Glazman, Phys. Rev. Lett. **93**, 196403 (2004).

[17] A. Crépieux, R. Guyon, P. Devillard, and T. Martin, Phys. Rev. B **67**, 205408 (2003).

[18] A. V. Lebedev, A. Crépieux, and T. Martin, Phys. Rev. B **71**, 075416 (2005).

[19] F. Wu, P. Queipo, T. Tsuneta, T. H. Wang, E. Kauppinen, and P. J. Hakonen, Phys. Rev. Lett. **99**, 156803 (2007).

[20] L. G. Herrmann, T. Delattre, P. Morfin, J.-M. Berroir, B. Plaçais, D. C. Glattli, and T. Kontos, Phys. Rev. Lett. **99**, 156804 (2007).

[21] H. Steinberg, G. Barak, A. Yacoby, L. N. Pfeiffer, K. W. West, B. I. Halperin, and K. Le Hur, Nat. Phys. **4**, 116 (2008).

[22] I. Safi and H. J. Schulz, Phys. Rev. B **52**, R17040 (1995).

[23] D. L. Maslov and M. Stone, Phys. Rev. B **52**, R5539 (1995); V. V. Ponomarenko, *ibid.* **52**, R8666 (1995).

[24] Due to the effectively short-ranged interaction induced by the gate, a Wigner crystal regime does not arise in the situation discussed here.

[25] C. S. Peça, L. Balents, and K. J. Wiese, Phys. Rev. B **68**, 205423 (2003).

[26] P. Recher, N. Y. Kim, and Y. Yamamoto, Phys. Rev. B **74**, 235438 (2006).

[27] K. Le Hur, B. I. Halperin, and A. Yacoby, Ann. Phys. (N.Y.) **323**, 3037 (2008).

[28] M. Büttiker, J. Phys.: Condens. Matter **5**, 9361 (1993).

[29] Here V_T is taken as an external parameter, and the choice of the value $\bar{V}_T$ ensures a vanishing average current I_T. The term "voltage probe" is sometimes also used in the literature for a terminal where the electrochemical potential dynamically changes to ensure that both the average current I_T and its current fluctuations vanish (see, e.g., Ref. 7). As far as the results for the average currents in the setup are concerned, our definition of a voltage probe is equivalent to the latter choice. Differences might emerge for the current fluctuations, which are beyond the topic of the present work.

[30] L. V. Keldysh, Zh. Eksp. Teor. Fiz. **47**, 1515 (1964).

[31] Note that the renormalization exhibits the same scaling exponent as in the homogeneous Luttinger liquid model [see, e.g., C. L. Kane and M. P. A. Fisher, Phys. Rev. B **46**, 15233 (1992)]. In the inhomogeneous Luttinger liquid model used here, however, the renormalization flow driven by the relevant impurity backscattering operator is cut not only by a finite temperature T or bias V but also by the finite length of the wire L. For this reason our perturbative treatment is safe also at $V=0$ and $T=0$.

[32] F. Dolcini, H. Grabert, I. Safi, and B. Trauzettel, Phys. Rev. Lett. **91**, 266402 (2003); F. Dolcini, B. Trauzettel, I. Safi, and H. Grabert, Phys. Rev. B **71**, 165309 (2005).

[33] P. Fendley, A. W. W. Ludwig, and H. Saleur, Phys. Rev. B **52**, 8934 (1995).

[34] R. Egger and H. Grabert, Phys. Rev. Lett. **79**, 3463 (1997).

[35] I. Safi, Ann. Phys. (Paris) **22**, 463 (1997) in French.

[36] K.-V. Pham, M. Gabay, and P. Lederer, Phys. Rev. B **61**, 16397 (2000); K.-I. Imura, K.-V. Pham, P. Lederer, and F. Piéchon, *ibid.* **66**, 035313 (2002).

[37] K. Le Hur, Phys. Rev. B **65**, 233314 (2002); Phys. Rev. Lett. **95**, 076801 (2005).

[38] See also M. P. A. Fisher and L. I. Glazman, in *Mesoscopic Electron Transport*, NATO ASI Series E 345, edited by L. L. Sohn, L. P. Kouwenhoven, and G. Schön (Kluwer Academic, Dordrecht, 1997).

[39] Y. V. Nazarov, A. A. Odintsov, and D. V. Averin, Europhys. Lett. **37**, 213 (1997).

[40] One can prove that only impurity backward scattering contributes to order $\gamma^2\lambda$.

[41] A. O. Gogolin, A. A. Nersesyan, and A. M. Tsvelik, *Bosonization and Strongly Correlated Systems* (Cambridge University Press, Cambridge, 1998).